![frontiers logo] Frontiers in Chemistry

Poly(aniline-*co*-melamine)@MnFe$_2$O$_4$ nanocatalyst for the synthesis of 4,4′-(arylmethylene) bis (1H-pyrazole-5-ol) derivatives, and 1,4-dihydropyrano[2,3-*c*]pyrazoles and evaluation of their antioxidant, and anticancer activities

Shefa Mirani Nezhad[1], Seied Ali Pourmousavi[1],
Ehsan Nazarzadeh Zare[1]*, Golnaz Heidari[1],
Hamed Manoochehri[2] and Esmaeel Sharifi[3]

[1]School of Chemistry, Damghan University, Damghan, Iran, [2]Research Center for Molecular Medicine,
Hamadan University of Medical Sciences, Hamadan, Iran, [3]Department of Tissue Engineering and
Biomaterials, School of Advanced Medical Sciences and Technologies, Hamadan University of Medical
Sciences, Hamadan, Iran

In this work, magnetic poly(aniline-*co*-melamine) nanocomposite as an efficient heterogeneous polymer-based nanocatalyst was fabricated in two steps. First, poly(aniline-*co*-melamine) was synthesized through the chemical oxidation by ammonium persulfate, then the magnetic nanocatalyst was successfully prepared from the *in-situ* coprecipitation method in the presence of poly(aniline-*co*-melamine). The resulting poly(aniline-*co*-melamine)@MnFe$_2$O$_4$ was characterized by FTIR, FESEM, XRD, VSM, EDX, TGA, and UV-vis analyses. The catalytic activity of poly(aniline-*co*-melamine)@MnFe$_2$O$_4$ was investigated in the synthesis of 4,4′-(arylmethylene)bis(1H-pyrazole-5-ol) derivatives, and new alkylene bridging bis 4,4′-(arylmethylene) bis(1H-pyrazole-5-ol) derivatives in excellent yields. The yield of 1,4-dihydropyrano[2,3-c]pyrazoles, 4,4′-(arylmethylene)bis(1H-pyrazol-5-ol), yields, and new alkylene bridging bis 4,4′-(arylmethylene)bis(1H-pyrazol-5-ol) derivatives were obtained 89%–96%, 90%–96%, and 92%–96%, respectively. The poly(aniline-*co*-melamine)@MnFe$_2$O$_4$ nanocatalyst can be recycled without pre-activation and reloaded up to five consecutive runs without a significant decrease in its efficiency. In addition, the antioxidant activity of some derivatives was evaluated by DPPH assay. Results showed that the maximum antioxidant activity of 4,4′-(arylmethylene)bis(1H-pyrazole-5-ol) derivatives and 1,4-dihydropyrano[2,3-*c*]pyrazoles were 75% and 90%, respectively. Furthermore, 4,4′-(arylmethylene)bis(1H-pyrazole-5-ol)

derivatives and 1,4-dihydropyrano[2,3-*c*]pyrazoles showed good potential for destroying colon cancer cell lines. Consequently, the poly(aniline-*co*-melamine)@MnFe$_2$O$_4$ nanocomposite is an excellent catalyst for green chemical processes owing to its high catalytic activity, stability, and reusability.

1 Introduction

Magnetic nanoparticles have been widely used as viable catalyst supports due to their high surface area, which results in high catalyst loading capacity, great dispersion, remarkable stability, and easy catalytic recycling (Zhu et al., 2010; Guo et al., 2021a; Lian et al., 2021; Soares et al., 2022). The recovery of catalysts from liquid-phase processes is significantly easier with magnetic separation than with cross-flow filtering and centrifugation (Gu et al., 2020; Dang et al., 2022; Xu et al., 2022). Additionally, except for those that are very corrosive or acidic, the particles' magnetic characteristics are persistent enough to withstand the majority of chemical conditions. Easy accessibility of reactants to the active sites is also possible since the catalysts are often bound to the surface of the magnetic nanoparticles (Stevens et al., 2005; Hassanzadeh-Afruzi et al., 2022; Movagharnezhad et al., 2022). Because of their electrical resistance, physical and magnetic characteristics, and great chemical stability, ferrites, a subclass of ferrimagnetic ceramics, are widely recognized (Alizadeh and Baseri, 2022). The spinel, hexagonal, and garnet structures of ferrites are determined by their original crystal lattice. The normal and inverse spinel ferrites are particularly appealing among these structures (Bououdina and Manoharan, 2020; Özdemir et al., 2020).

Superparamagnetism, single domain effects, high coercivity, moderate magnetization, and spin-filtering are just a few of the distinctive magnetic properties that make it possible for magnetic transition oxide nanostructures with spinel structure MFe$_2$O$_4$ (M = Ni, Co, Fe, Mn, etc.) to have remarkable biological and industrial functionalities (Zipare et al., 2015). Due to its captivating electromagnetic and magnetic characteristics, as a significant member of the ferrite family, MnFe$_2$O$_4$ (MFO) has garnered significant study attention. As MnFe$_2$O$_4$ is partly inverse spinel, about 80% of Mn^{2+} ions are found at the tetrahedral site, while just 20% are found at the octahedral site (Deraz and Alarifi, 2012). The features of MnFe$_2$O$_4$ nanoparticles and thin films are varied, including high curie temperature, superparamagnetism, super spin glass state, size-dependent saturation magnetization, and high anisotropy constant (Carta et al., 2010). The magnetic nanoparticles such as MnFe$_2$O$_4$, MgFe$_2$O$_4$, CoFe$_2$O$_4$, ZnFe$_2$O$_4$, Fe$_3$O$_4$, and their nanocomposites due to their biocompatibility, good physicochemical properties and small particle size have several applications in targeted drug delivery, magnetic resonance imaging (MRI), mediators for hyperthermia applications, etc., (Islam et al., 2020).

The magnetic particles are rarely used in their unprocessed form; instead, they are often mixed with an organic polymer matrix or an inorganic silica carrier and placed in a liquid media to prevent aggregation (Guo et al., 2021b; Jazzar et al., 2021). The particles are endowed with organic polymers with the functional groups required for the desired uses (Kalia et al., 2014). This combination of organic polymers and magnetic nanoparticles provides a diverse range of opportunities for the creation of a new class of organic/inorganic hybrid materials that have dual properties. The resulting magnetic polymers have shown to be helpful for a range of purposes since they combine magnetic characteristics with high stability and reputable biocompatibility. The polymer nanocomposites due to high functionality, good phsicochmichal proprtes, and biocompatibility have received increasing attention in biomedical applications (Hule and Pochan, 2007). Thus, they've been used effectively in new applications including hyperthermia, bioseparation, medication delivery, targeted oil recovery, and so on (Philippova et al., 2011). Nevertheless, since magnetic nanoparticles possess a high surface-area-to-volume ratio and are scattered in a polymer matrix, it is difficult to create magnetic polymer nanocomposites that have a consistent magnetic field equivalent to that of an inorganic magnetic material. It is commonly known that a particle's magnetic properties depend on its chemical composition, shape, size, and surface characteristics. To determine the sorts of applications appropriate for polymer usage, precise control of the aforementioned factors is required. The creation of magnetic polymer nanocomposites has been investigated using a variety of methods, including simultaneous formation of polymers and particles, polymerization of monomers with the presence of particles, *in-situ* formation of particles into preformed polymers, and direct mixing (Massart, 1981; Jazzar et al., 2021).

Pyrazoles, commonly known as azoles, are five-membered ring heterocyclic compounds that include two nitrogen atoms in neighboring locations (Parajuli et al., 2013). Treatment of inflammation and illnesses linked to inflammation, such as arthritis, is the most well-known use of nearly every category of pyrazoles. Pyrazoles are the focus of numerous investigations due to their broad range of biological potential activities, including anticancer, anti-inflammatory (Amir et al., 2008),

antihistaminic (Yildirim et al., 2005), antitumor (Park et al., 2005), antiviral (Larsen et al., 1999), anti-diabetic, anticonvulsant, and antimicrobial (Pimenova and Voronina, 2001) activities. Ethylacetoacetate and substituted hydrazine are typically used as the starting materials when synthesizing pyrazolone. With the aid of numerous catalysts, the production of pyrazoles has been reported to employ a variety of techniques and conditions. For example, pyrazolo[3,4-b]pyridine-5-carboxamide derivatives were catalyzed by p-toluenesulfonic acid under mild reaction conditions and in good yields at ambient temperature (Shaabani et al., 2009), Poly(ethylene imine)-modified magnetic halloysite nanotubes was used as a catalyst for the synthesis of dihydropyrano[2,3-c] pyrazole derivatives (Hajizadeh and Maleki, 2018).

In this study, we focused on fabricating magnetic poly(aniline-*co*-melamine)@MnFe$_2$O$_4$ nanocomposite as a catalyst for the syntheses of 1,4-dihydropyrano[2,3-*c*]pyrazoles and synthesis of 4,4′-(arylmethylene)bis(1H-pyrazole-5-ols). These compounds were also tested for antioxidant and anticancer activities.

2 Experimental section

2.1 Materials and methods

Aniline, melamine, ferric chloride (FeCl$_3$·6H$_2$O), ammonium persulfate, manganese (II) chloride (MnCl$_2$.2H$_2$O), sodium hydroxide, solvents, and all other reagents were purchased from Merck Company, Germany.

2.2 Preparation of poly(aniline-*co*-melamine)@MnFe$_2$O$_4$ nanocatalyst

To 40 ml of HCl (1 M), 1 ml aniline and 1.38 g melamine were added. The reaction mixture was stirred at 50°C until the melamine was entirely dissolved and was kept at 0°C–4°C under an inerth atmosphere. Then, 20 ml of ammonium persulfate solution (6.02 g) was added dropwise to the above solution. The reaction was maintained at 0°C–4°C for 12 h. The dark green poly(aniline-*co*-melamine) precipitate was then recovered by filtering and washed multiple times using water and methanol to eliminate the residual oxidizing agent and oligomers. The cleansed product was submerged in boiling water for 20 min and agitated to thoroughly dissolve the undissolved melamine. The *in-situ* co-precipitation method was used for the preparation of poly(aniline-*co*-melamine)@MnFe$_2$O$_4$ nanocomposite as follows:

0.33 g of MnCl$_2$.2H$_2$O and 0.5 g of FeCl$_3$.6H$_2$O were dissolved in 25 ml of deionized water. The solution was then mixed with 1 g of poly(aniline-*co*-melamine) at 80°C for 20 min. The mixture was treated with a 1 M NaOH solution until the pH reached 12. After 3 h, the black precipitate was magnetically

separated and repeatedly rinsed with deionized water and ethanol and drided at 40°C in the vacuum oven for 10 h. Figure 1A shows the reaction steps for the preparation of the nanocomposite.

2.3 General procedure for the synthesis of 3-methyl-1-phenyl-1H-pyrazole-5-ol

For the synthesis of 3-methyl-1-phenyl-1H-pyrazole-5-ol, phenylhydrazine (0.05 mol, 5 ml), acetic acid (0.5 ml), and ethyl acetoacetate (0.05 mol, 6.2 ml) were stirred in the reaction vessel at 90°C for 1 hour. After cooling at room temperature, 10–20 ml ether was added to the mixture the precipitate was filtered, and the product was crystallized using ethanol (Nezhad et al., 2022).

2.4 General procedure for the synthesis of 1,4-dihydropyrano[2,3-*c*]pyrazole derivatives

A mixture of 3-methyl-1-phenyl-1*H*-pyrazole-5-ol (1 mmol), an aldehyde (1.0 mmol), malononitrile (1 mmol), and poly(aniline-*co*-melamine)@MnFe$_2$O$_4$ nanocomposite (0.05 g) in water/EtOH (5 ml 1:1) was stirred at 40°C until the reaction was complete. The completion of the reaction was monitored by thin-layer chromatography (hexane/ethyl acetate 4:1). To the separation of the product, the catalyst was separated by an external magnet and the crude solid product was filtered and washed three times with ethanol (Figure 1B).

2.5 General procedure for the synthesis of 4,4′-(arylmethylene)bis(1H-pyrazole-5-ol) derivatives

3-methyl-1-phenyl-1H-pyrazole-5-ol (2 mmol), an aldehyde (1.0 mmol), and poly(aniline-*co*-melamine)@MnFe$_2$O$_4$ nanocomposite (0.05 g) were mixed, and the reaction was stirred at room temperature to finished. An external magnet was used to isolate the catalyst. The unpurified solid product was filtered, then refined using water and ethanol recrystallization (50:50) (Figure 1C).

2.6 General procedure for the synthesis of bis 4,4′-(arylmethylene)bis(1H-pyrazole-5-ol) derivatives

3-methyl-1-phenyl-1H-pyrazole-5-ol (2 mmol), an aldehyde (0.5 mmol), and poly(aniline-*co*-melamine)@MnFe$_2$O$_4$ nanocomposite (0.05 g) were mixed, and the reaction was stirred at room temperature to finished. An external magnet

FIGURE 1
Preparation of poly(aniline-*co*-melamine)@MnFe$_2$O$_4$ nanocomposite in two steps **(A)**, synthesis of 1,4-dihydropyrano[2,3-*c*]pyrazoles **(B)**, synthesis of 4,4′-(arylmethylene)bis(1H-pyrazole–5-ol) derivatives **(C)**, and synthesis of bis 4,4′-(arylmethylene)bis(1H-pyrazole–5-ol) derivatives **(D)**.
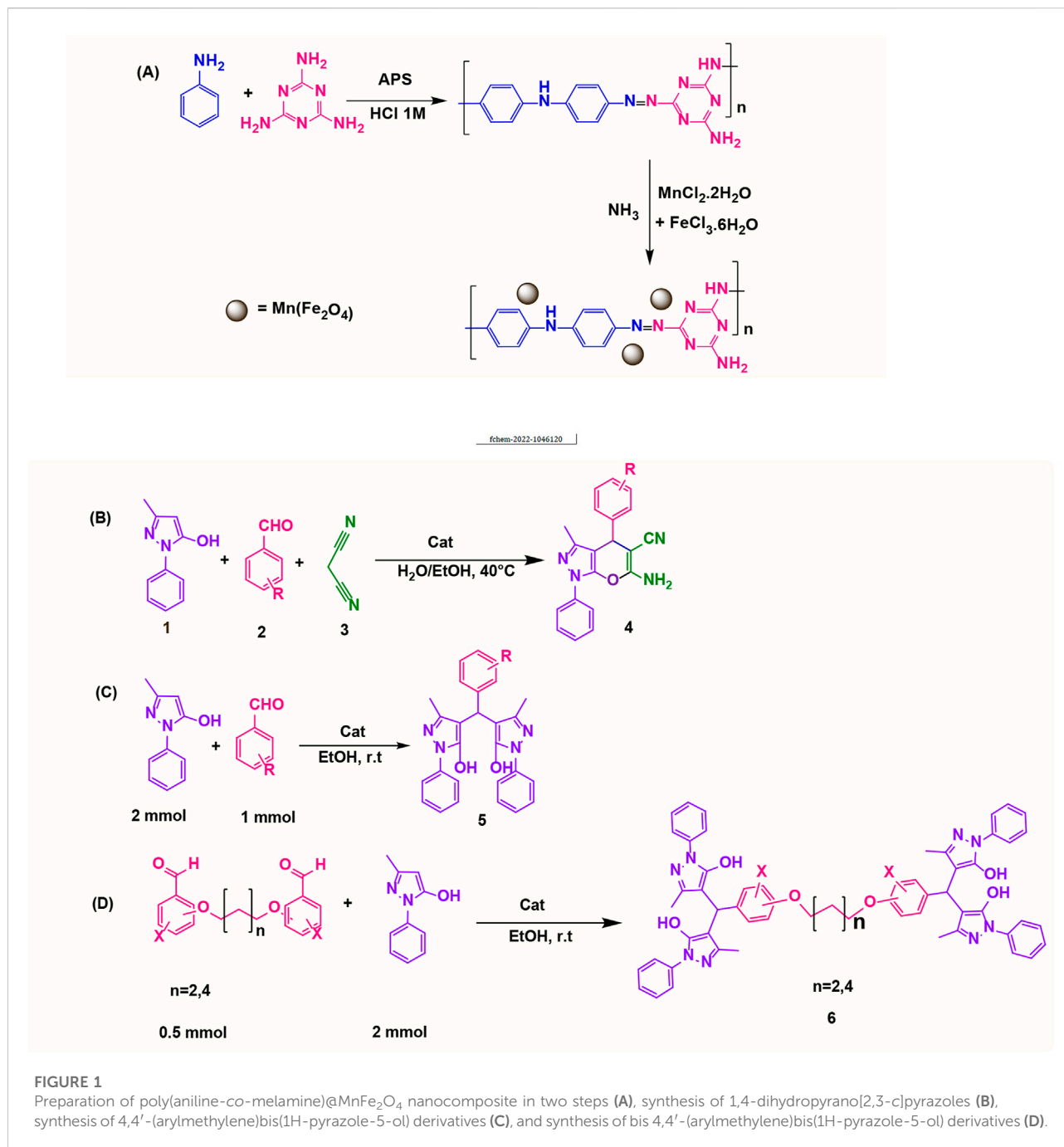
was used to isolate the catalyst. The crude solid product was filtered and washed three times with ethanol (Figure 1D).

2.7 Antioxidant activity

The antioxidant activity of 1,4-dihydropyrano[2,3-*c*] pyrazoles (4q, 4d, 4o, 4l), 4,4′-(arylmethylene)bis(1H-pyrazole-5-ol) (5i, 5j, 5q), bis 4,4′-(arylmethylene)bis(3-methyl-1H-pyrazol-5-ols) (6c) derivative was evaluated by DPPH (2,2-diphenyl-1-picrylhydrazyl) radical scavenger assy. Accordingly, derivatives were examined for their ability to the bleaching of the purple-colored ethanol solution DPPH. 100 mg of each sample was reacted with 1 ml of ethanolic DPPH at room temperature. Afterward, the absorbance of the reaction mixture was measured at 517 nm and the inhibition percentage was evaluated by the following formula (Ghahremanloo et al., 2022): DPPH inhibition (%) = A_b-A_s/A_b ×100.

FIGURE 2
FTIR spectra of the prepared MnFe$_2$O$_4$ **(A)**, poly(aniline-*co*-melamine) **(B)**, and poly(aniline-*co*-melamine) @MnFe$_2$O$_4$ **(C)**

FIGURE 3
XRD patterns of the prepared MnFe$_2$O$_4$ **(A)**, poly(aniline-*co*-melamine) **(B)**, and poly(aniline-*co*-melamine) @MnFe$_2$O$_4$ **(C)**.
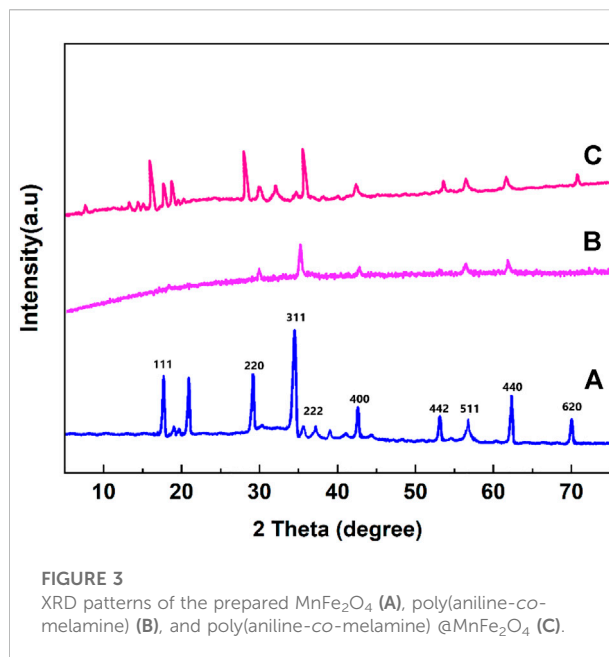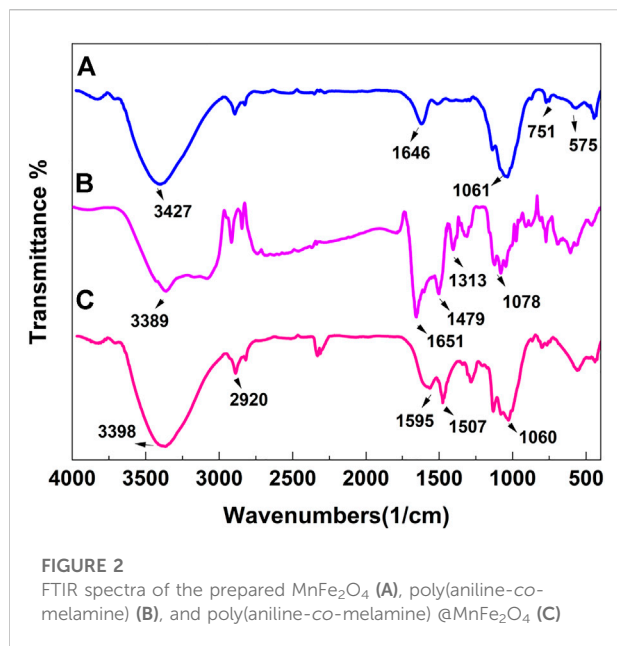
2.8 *In-vitro* anticancer study

The anti-cancer activity of 1,4-dihydropyrano[2,3-*c*] pyrazoles (4q, 4d, 4o, 4l), 4,4′-(arylmethylene)bis(1H-pyrazole-5-ol) (5i, 5j, 5q), bis 4,4'-(arylmethylene)bis(3-methyl-1H-pyrazole-5-ols) (6c) derivative was investigated by MTT assay. Briefly, 3,000 cells (HCT116 as the human colon cancer cell line and L929 as the normal cell line) were seeded in 96 well culture plates. After attachment, cells were treated with 4q, 4d, 4o, 4l, 5i, 5j, 5j, 5q and 6c (12.5–200 ug/mL). In the time points of 24 and 48 h after treatment, MTT dye (0.5 mg/ml) was added to each well. Plates were incubated at 37°C for 4 h, the cultured medium was withdrawn and 100 µl of DMSO was added to each well. Plates were shaken for 20 min and their absorbance was read at 570 nm using a plate reader. The viability of treated cells was calculated by the following formula (Hu et al., 2019): Viability (%) (Absorbance of treated cells/Absorbance of control cells) × 100.

2.9 Characterization

Fourier transform infrared spectroscopy (FTIR, Bruker Tensor 27, Bremen, Germany), hydrogen and carbon nuclear magnetic resonance spectroscopy (^{1}HNMR and ^{13}CNMR, Bruker Avance DRX-400, Bremen, Germany) were employed for the chemical characterization of the products. The crystallinity and surface morphology of samples were investigated by X-ray diffraction (XRD, Shibuya-ku, Tokyo, Japan) and field emission scanning electron microscope (FESEM, Hitachi S4160 instrument, Japan), energy dispersive X-ray analysis

(EDX, MFTIRA III, TESCAN, Czech Republic), respectively. Thermogravimetric analysis (TGA 209F3, NETZSCH, Selb, Germany) was utilized to test the thermal stability of samples.

3 Results and discussions

3.1 Characterization of polymer-based nanocatalyst

3.1.1 Fourier transform infrared spectroscopy

The FTIR absorption spectra of the prepared MnFe$_2$O$_4$ (a), poly(aniline-*co*-melamine) (b), poly(aniline-*co*-melamine) @MnFe$_2$O$_4$ (c) nanocomposite are shown in Figure 2. The MnFe$_2$O$_4$ spectrum exhibits two prominent absorption bands below 1,000 cm^{-1}, which is a characteristic of ferrites. The distinctive bands at 449 and 573 cm^{-1} are caused by the metal-inherent oxygen's stretching vibrations at the octahedral and tetrahedral sites, respectively (Zipare et al., 2015). The poly(aniline-*co*-melamine) (b) and poly(aniline-*co*-melamine)@MnFe$_2$O$_4$ (c) samples displayed very similar spectra. The stretching vibration of the NH$_2$ and N-H groups is observed at 3,390 cm^{-1}. The stretching modes of benzenoid amine and quinoid imine units, respectively, are associated with the two distinctive bands at around 1,500 and 1,600 cm^{-1}. The vibrations of the C-H and C-N stretching bonds in the benzene ring are responsible for the peaks at 1,106 and 1,296 cm^{-1}, respectively. The band corresponding to the bending vibrations of the C-H bond in the p-disubstituted benzene rings can be seen in the 797 cm^{-1} (Maroufi et al., 2020).
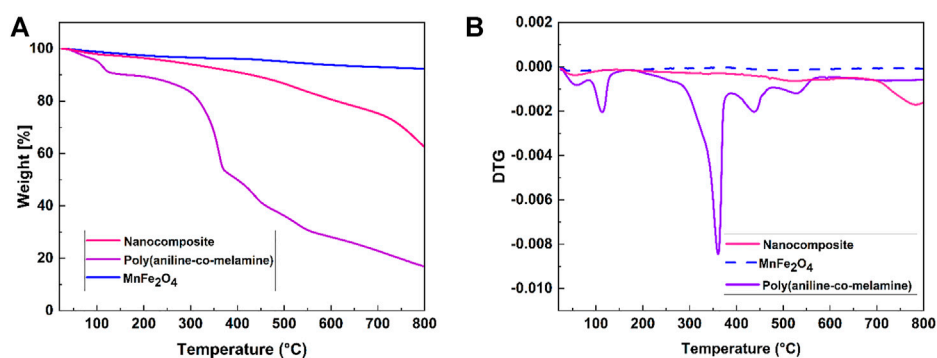
FIGURE 4
TGA **(A)**, and DTG thermograms **(B)** of the prepared $MnFe_2O_4$, poly(aniline-*co*-melamine), and poly(aniline-*co*-melamine) @$MnFe_2O_4$.
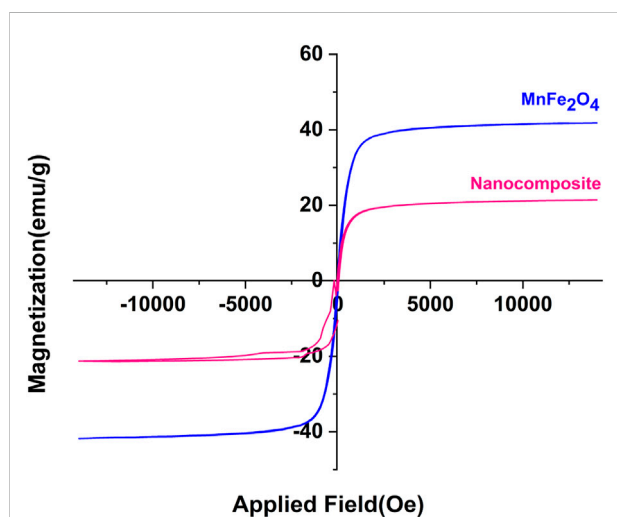
FIGURE 5
VSM curves of the prepared $MnFe_2O_4$ and poly(aniline-*co*-melamine)@$MnFe_2O_4$.
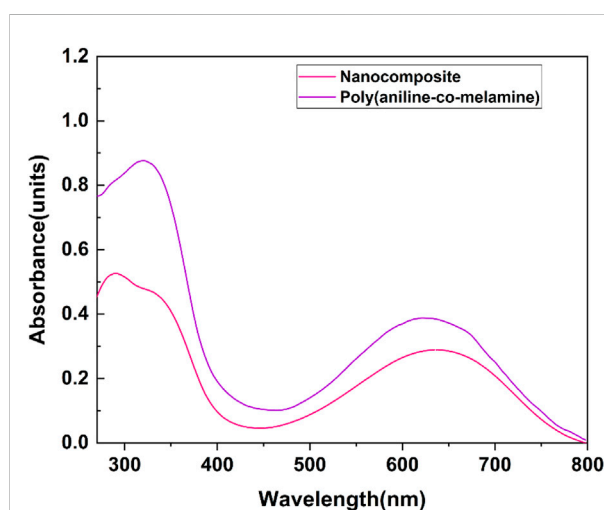
FIGURE 6
UV-vis absorption spectra of poly(aniline-*co*-melamine) and poly(aniline-*co*-melamine)@$MnFe_2O_4$ in DMSO solvent.

3.1.2 X-ray diffraction

XRD patterns of the prepared $MnFe_2O_4$, poly(aniline-*co*-melamine), poly(aniline-*co*-melamine)@$MnFe_2O_4$ nanocomposite are shown in Figure 3. The XRD pattern of $MnFe_2O_4$ nanoparticles revealed a crystalline character. This pattern reveal the typical diffraction peaks of the $MnFe_2O_4$ nanoparticles at 18.10°, 30.60°, 36.15°, 43.65°, 54.10°, 57.65°, and 63.25° are attributable to the crystal planes of (111), (220), (311), (400), (422), (511), (440), and (620) respectively (Qin et al., 2021). The XRD patterns of the poly(aniline-*co*-melamine) (b) and (polyaniline-*co*-melamine)@$MnFe_2O_4$ nanocomposite (c) showed a semicrystalline nature. The existence of corresponding peaks of $MnFe_2O_4$ and poly(aniline-*co*-

melamine) approved the successful preparation of the nanocomposite.

3.1.3 Thermogravimetric analysis

The TG/DTG curves of the $MnFe_2O_4$, poly(aniline-*co*-melamine), and poly(aniline-*co*-melamine)@$MnFe_2O_4$ nanocomposite are given in Figures 4A,B. The weight loss (below 150°C) observed in the TG curve of $MnFe_2O_4$ is related to the evaporation of adsorbed water on the surface of the nanoparticles. Three weight losses are observed in the TG curve of poly(aniline-*co*-melamine). The first step of degradation between 80°C and 200°C corresponded to theremoval of water. The second and
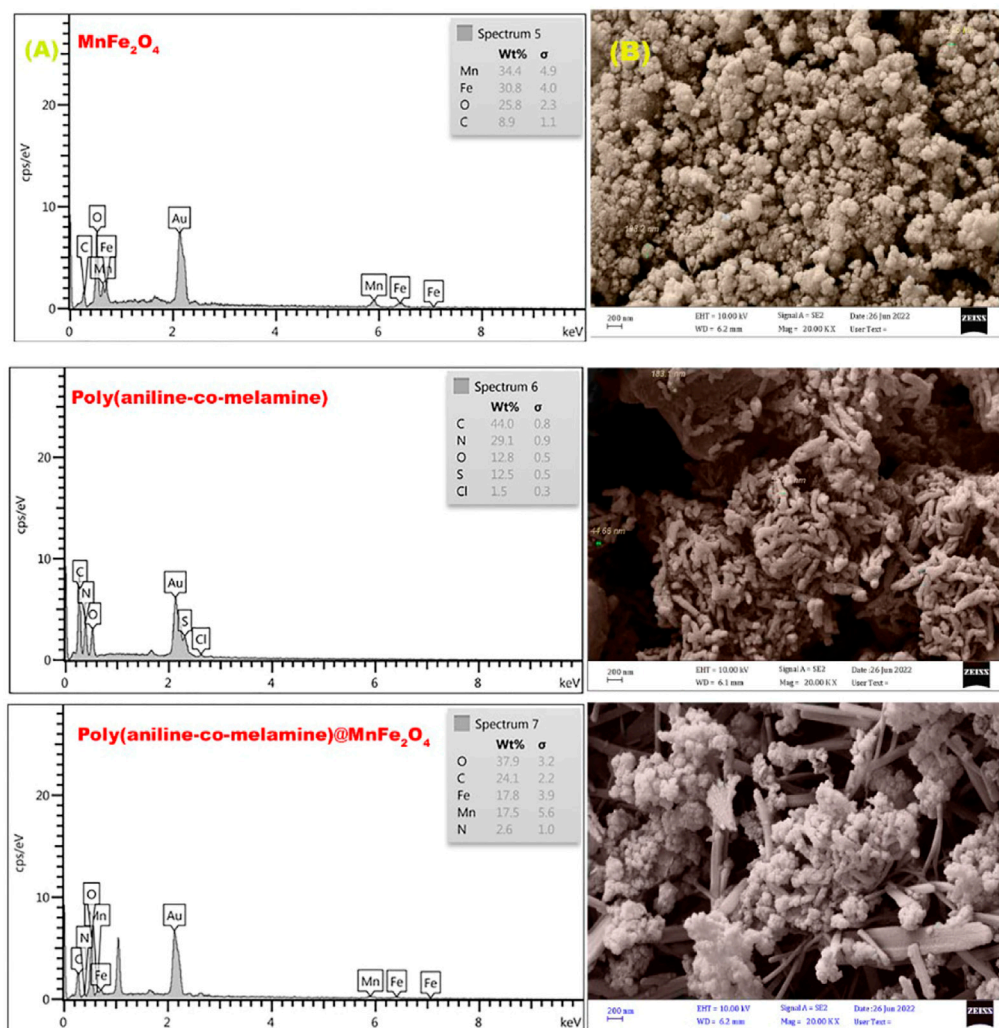
FIGURE 7
EDX spectra **(A)**, and FESEM micrographs **(B)** of the prepared MnFe$_2$O$_4$, poly(aniline-*co*-melamine), and poly(aniline-*co*-melamine) @MnFe$_2$O$_4$ nanocomposite.

third weight losses at 210°C and up to 800°C are related to the melamine breakdown and minor degradation of polymeric chains, respectively (Maroufi et al., 2020). The comparison of TG curves of poly(aniline-*co*-melamine)and poly(aniline-*co*-melamine)@MnFe$_2$O$_4$ nanocomposite showed that the stability of poly(aniline-*co*-melamine)@MnFe$_2$O$_4$ nanocomposite was higher than the poly(aniline-*co*-melamine).

3.1.4 VSM

The VSM curves of the poly(aniline-*co*-melamine) @MnFe$_2$O$_4$ nanocomposite and MnFe$_2$O$_4$ are revealed in Figure 5. The VSM curves show that the magnetization saturation values of MnFe$_2$O$_4$ nanoparticles and poly(aniline-*co*-melamine)@MnFe$_2$O$_4$ were 21.28 and

41.81 emu/g, respectively. In addition, the magnetic property of the nanocomposite was lower than the MnFe$_2$O$_4$ nanoparticles. This could be related to covering the magnetic nanoparticles with poly(aniline-*co*-melamine) copolymer.

3.1.5 UV-vis

The UV–vis absorption spectra of poly(aniline-*co*-melamine), and poly(aniline-*co*-melamine)@MnFe$_2$O$_4$ are presented in Figure 6. A specific DMSO concentration was used to evaluate both samples. The UV–vis spectrum of poly(aniline-*co*-melamine) shows two characteristic absorption peaks assigned to the n-π* and π–π* electron transition within the benzenoid segments in the range of 300–400 nm. A charge transfer from the benzenoid rings to the quinoid rings causes the

TABLE 1 Optimization of the three-component reaction of 3-methyl-1-phenyl-1*H*-pyrazole-5-ol, benzaldehyde, and malononitrile under various conditions.[a]

Entry	Solvent	Catalyst (g)	Temp/°C	Time/min	Yield%[b]
1	EtOH/H$_2$O	Catalyst 0.04	40	35	85
2	H$_2$O	Catalyst 0.04	40	60	50
3	THF	Catalyst 0.04	40	120	35
4	EtOH	Catalyst 0.04	40	60	60
5	CHCl$_3$	Catalyst 0.04	40	120	45
6	Solvent-free	Catalyst 0.04	100	120	55
7	EtOH/H$_2$O	Catalyst 0.04	60	30	65
8	EtOH/H$_2$O	Catalyst 0.04	Reflux	60	60
9	EtOH/H$_2$O	Catalyst 0.04	r.t	60	55
10	EtOH/H$_2$O	Catalyst 0.03	40	50	80
11	**EtOH/H$_2$O**	**Catalyst 0.05**	**40**	**20**	**90**
11	EtOH/H$_2$O	Catalyst 0.06	40	20	90
12	EtOH/H$_2$O	—	40	120	50
13	EtOH/H$_2$O	Poly(aniline-*co*-melamine) 0.05	40	15	90
14	EtOH/H$_2$O	MnFe$_2$O$_4$ 0.05	40	60	50

[a]Reaction conditions: aldehyde (1 mmol), 3-methyl-1-phenyl-1*H*-pyrazol-5-ol (1 mmol), and malononitrile (1 mmol).
[b]Isolated yield.
The bold value row showed the best condition.

absorption peak at roughly 620 nm (Maroufi et al., 2020). The presence of MnFe$_2$O$_4$ in the nanocomposite leads to reducing in the solubility of the poly(aniline-*co*-melamine)@MnFe$_2$O$_4$. The UV–vis absorption spectrum of poly(aniline-*co*-melamine)@MnFe$_2$O$_4$ is weaker than the UV–vis spectrum of poly(aniline-*co*-melamine).

3.1.6 Field emission scanning electron microscope

Figure 7A displays the FESEM images of MnFe$_2$O$_4$, poly(aniline-*co*-melamine), and poly(aniline-*co*-melamine)@MnFe$_2$O$_4$ in magnifications of 200 nm. The average particle size for the of MnFe$_2$O$_4$ was 60 nm, The FESEM image of poly(aniline-*co*-melamine) showed rod-like structure with a diameter of 44–183 nm. The FESEM image of poly(aniline-*co*-melamine)@MnFe$_2$O$_4$ show the particle size decreased after the composite was prepared. The average particle size diameter was 50 nm. These findings revealed that The FESEM image of the nanocomposite was successfully prepared.

3.1.7 Energy dispersive X-ray analysis

As shown in Figure 7B, the chemical composition of the produced MnFe$_2$O$_4$, poly(aniline-*co*-melamine), and poly(aniline-*co*-melamine) @MnFe$_2$O$_4$ was also determined using the EDXanalysis. The presence of various quantities of O, C, N, Mn, and Fe elements was proven by comparing spectra and tabular data. The occurrence of S and Cl in poly(aniline-*co*-melamine) is related to ammonium persulfate and HCl trapped in the polymer matrix.

3.2 Evaluation of the catalytic activity of poly(aniline-*co*-melamine)@MnFe$_2$O$_4$ nanocomposite through the synthesis of 1,4-dihydropyrano[2,3-*c*]pyrazole derivatives

To test the catalytic activity of poly(aniline-*co*-melamine)@Mn(Fe$_2$O$_4$), first the synthesis of 1,4-dihydropyrano[2,3-*c*] pyrazoles utilizing aromatic aldehyde, 3-methyl-1-phenyl-1H-pyrazole-5-ol, and malononitrile were carried out (Figure 1B).

The reaction conditions of benzaldehyde, 3-methyl-1-phenyl-1H-pyrazole-5-ol, and malononitrile in the presence of poly(aniline-*co*-melamine)@MnFe$_2$O$_4$ as a catalyst were optimized to get a higher yield. Following that, a solvent screening indicated that the reaction was more successful in water and ethanol. When benzaldehyde (1 mmol), and 3-methyl-1-phenyl-1*H*-pyrazole-5-ol (1 mmol) were reacted with malononitrile (1 mmol) in the presence of Poly(aniline-*co*-melamine)@MnFe$_2$O$_4$ (0.05 g) in Ethanol/H$_2$O (1:1) at 40°C, the best results were attained (Table 1 entry 11). On the other hand, it is confirmed that the reaction requires a catalyst to continue and that the efficiency is not high in the absence of a catalyst (Table 1, entry 12). In this reaction model, the conversion rates were examined in the presence of poly(aniline-*co*-melamine) and MnFe$_2$O$_4$ (Table 1, entries 13, 14), the results showing that the best result has been achieved in poly(aniline-*co*-melamine) but the major problem of poly(aniline-*co*-melamine) as a catalyst is easy solubility in organic solvents, and therefore its isolation is difficult. The poly(aniline-*co*-melamine)@MnFe$_2$O$_4$

TABLE 2 Synthesis of 1,4-dihydropyrano[2,3-*c*]pyrazoles by poly(aniline-*co*-melamine)@MnFe$_2$O$_4$ and benzaldehyde derivatives.[a]

Entry	Product	Code	Time. min	Yield %	TON	TOF X 10^{-3}(h^{-1})	M.P/°C		Ref
							Observed	Reported	
1		4a	20	90	3,333	10.1	169–172	168–169	Vafajoo et al. (2015)
2		4b	15	95	3,518	14.0	172–173	174–176	Vafajoo et al. (2015)
3		4c	25	91	3,370	8.2	173–175	172–173	Vafajoo et al. (2015)
4		4d	15	90	3,333	13.3	170–173	172–174	Vafajoo et al. (2015)
5		4e	10	93	3,444	20.7	192–193	190–195	Vafajoo et al. (2015)
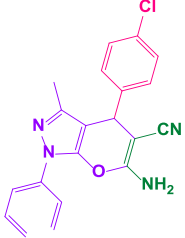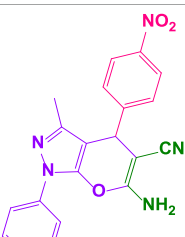
(Continued on following page)

TABLE 2 (*Continued*) Synthesis of 1,4-dihydropyrano[2,3-*c*]pyrazoles by poly(aniline-*co*-melamine)@MnFe$_2$O$_4$ and benzaldehyde derivatives.[a]

Entry	Product	Code	Time. min	Yield %	TON	TOF X $10^{-3}(h^{-1})$	M.P/°C		Ref
							Observed	Reported	
6		4f	15	92	3,407	13.6	189–191	190–192	Vafajoo et al. (2015)
7		4g	20	89	3,269	9.9	202–204	200–203	Jasim et al. (2022)
8		4h	25	90	3,333	8.1	196–198	193–195	Vafajoo et al. (2015)
9		4i	25	93	3,444	8.4	191–193	193–195	Zolfigol et al. (2016)
10		4j	25	92	3,407	8.3	172–173	169–171	Vafajoo et al. (2015)
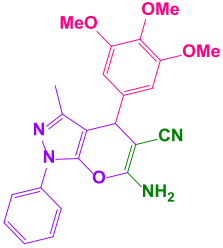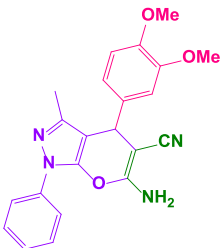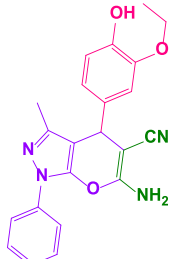
(Continued on following page)

TABLE 2 (*Continued*) Synthesis of 1,4-dihydropyrano[2,3-*c*]pyrazoles by poly(aniline-*co*-melamine)@MnFe$_2$O$_4$ and benzaldehyde derivatives.[a]

Entry	Product	Code	Time. min	Yield %	TON	TOF X 10^{-3}(h^{-1})	M.P/°C		Ref
							Observed	Reported	
11		4k	15	95	3,518	14.0	240–242	244–245	Zolfigol et al. (2016)
12		4l	10	96	3,555	21.04	179–181	180–182	Vafajoo et al. (2015)
13		4m	15	90	3,333	13.3	147–149	145–146	Vafajoo et al. (2015)
14		4n	30	90	3,333	6.6	233–235	236–238	Vafajoo et al. (2015)
15		4o	30	90	3,333	6.6	168–170	167–168	Zolfigol et al. (2016)
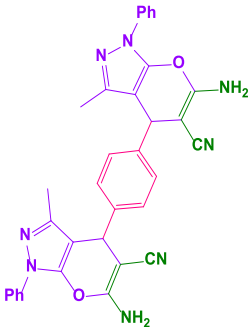
(Continued on following page)

TABLE 2 (*Continued*) Synthesis of 1,4-dihydropyrano[2,3-*c*]pyrazoles by poly(aniline-*co*-melamine)@MnFe$_2$O$_4$ and benzaldehyde derivatives.[a]

Entry	Product	Code	Time. min	Yield %	TON	TOF X 10^{-3}(h^{-1})	M.P/°C		Ref
							Observed	Reported	
16		4p	30	94	3,481	6.9	212–213	211–213	Vafajoo et al. (2015)
17		4q	35	90	3,333	5.7	208–209		
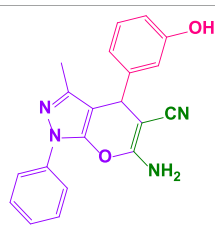
[a]Reaction conditions: aldehyde (1 mmol), 3-methyl-1-phenyl-1*H*-pyrazol-5-ol (1 mmol), and malononitrile (1 mmol), 5 ml water/EtOH (1:1) and poly(aniline-*co*-melamine)@MnFe$_2$O$_4$ (0.05) at 40°C.
The bold value row showed the best condition.
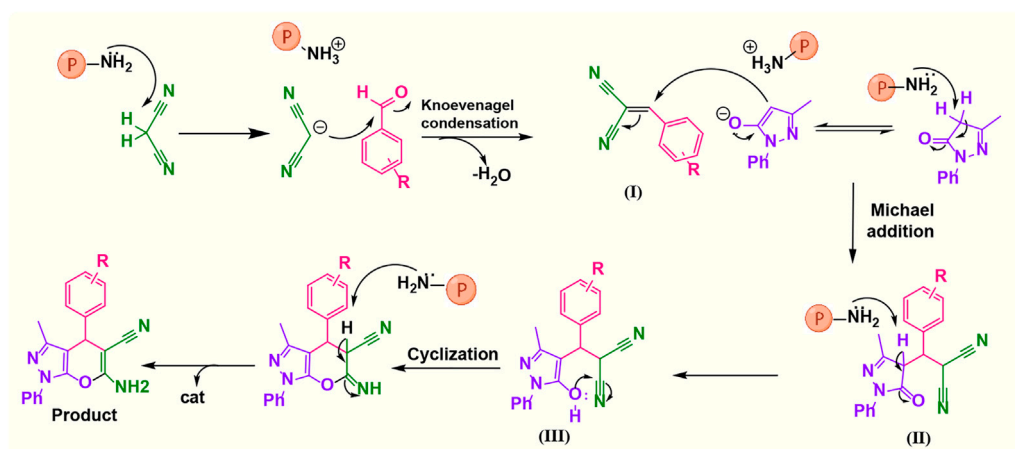
FIGURE 8
Suggested mechanistic scheme for the synthesis of 1,4-dihydropyrano[2,3-*c*]pyrazole catalyzed by poly(aniline-*co*-melamine)@Mn(Fe$_2$O$_4$). ℗ represents a polymer-based catalyst.

nanocomposite was consequently chosen as an efficient catalyst to carry out the reactions.

Obtained data from Table 1 showed that the catalytic activity of poly(aniline-*co*-melamine)@MnFe$_2$O$_4$ nanocomposite is higher compared to poly(aniline-*co*-melamine) and MnFe$_2$O$_4$. This result can be explained according to FESEM images. In the

FESEM images particle size in the poly(aniline-*co*-melamine) @MnFe$_2$O$_4$ nanocomposite is smaller than the poly(aniline-*co*-melamine) and larger than the MnFe$_2$O$_4$ nanoparticles. In addition, the morphology of nanocomposite is different from MnFe$_2$O$_4$ nanoparticles and poly(aniline-co-melamine) which showed agglomerate particles with disordered rod-like

TABLE 3 Optimization of the reaction of 3-methyl-1-phenyl-1H-pyrazol-5-ol, and benzaldehyde, under various conditions[a].

Entry	Solvent	Catalyst	Temp/°C	Time/min	Yield%[b]
1	EtOH/H$_2$O	0.05	50	30	70
2	H$_2$O	0.05	50	45	60
3	THF	0.05	50	100	30
4	EtOH	0.05	50	30	80
5	CHCl$_3$	0.05	50	100	50
6	Solvent-free	0.05	50	100	70
7	EtOH	0.05	80	30	60
8	EtOH	0.05	r.t	20	95
9	EtOH	0.04	r.t	35	85
10	EtOH	0.07	r.t	20	96

[a]Reaction conditions: aldehyde (1 mmol), 3-methyl-1-phenyl-1H-pyrazol-5-ol (2 mmol).
[b]Isolated yield.

structures. This observation showed that the presence of MnFe$_2$O$_4$ nanoparticles in the copolymer matrix led to decreasing the particle size and differencing in the morphology of the nanocomposite. It is well known that particle size and morphology are two important parameters that influence the catalytic performance of nanocatalysts (Kamalzare, 2022). Nanocatalysts with a high surface area could provide more active sites to less activation energy for catalytic reactions, and novel surface structures lead to product selectivity and catalytic efficacy. Thus, the higher catalytic activity of nanocomposite can be related to the high volume-to-surface ratio and different morphology of the nanocomposite.

The reaction with several aromatic aldehydes to yield a wide range of 1, 4-dihydropyrano[2,3-c]pyrazoles were examined in the terms of substrate scope (Table 2). The presence of poly(aniline-co-melamine)@MnFe$_2$O$_4$ revealed that this reaction is generally tolerable to a wide range of benzaldehyde derivatives comprising electron-withdrawing and electron-donating groups (0.05 g). Calculation of turnover number (TON) and turnover frequencies (TOF) provides a comprehensive way to make comparisons based on a per active site basis. These values have been calculated from the EDX and TGA data. The results are shown in Table 2 (Al-Hasani et al., 2017; Molaei and Javanshir, 2018).

3.2.1 Suggested mechanism

A possible mechanism (Figure 8) involves the initial activation of malononitrile using the catalyst and then attacking the carbonyl group of the aldehyde. By removing one water molecule, intermediate (I) is prepared (Knoevenagel condensation). The reaction is followed by deprotonation of 3-methyl-1-phenyl-1H-pyrazole-5-ol by a catalyst. Then, Michael's addition of 3-methyl-1-phenyl-

1H-pyrazole-5-ol to intermediate (I) affords (II). Intermediate (II) was converted to (III) via tautomerization, and the product is obtained by cyclization (Hajizadeh and Maleki, 2018).

The poly(aniline-co-melamine)@MnFe$_2$O$_4$ was employed also as a catalyst in the synthesis of bis pyrazolone. We investigated the synthesis of bispyrazolones using aromatic aldehyde (1 mmol) and 3-methyl-1-phenyl-1H-pyrazole-5-ol (2 mmol) (Figure 1C). In order to optimize this reaction, benzaldehyde and 3-methyl-1-phenyl-1H-pyrazole-5-ol were selected as starting materials, and the effects of temperature, amount of catalyst, solvent, etc., were investigated. The influence of varied quantities of catalysts on the reaction result was examined. Among different catalyst loadings (e.g., 0.04, 0.05, and 0.06 g), the catalyst based on poly(aniline-co-melamine) @MnFe$_2$O$_4$ (0.05 g) was selected as the most effective amount. Following that, it was investigated how the solvent affected the reaction's result. According to the data, ethanol was the best solvent for this kind of domino reaction. The findings of the subsequent investigation into the impact of temperature showed that room temperature conditions produced the product with the highest yield (Table 3).

Different electron-withdrawing or electron-donating groups, such as OCH$_3$, NO$_2$, and CH$_3$, were chosen to react with 3-Methyl-1H-phenyl-5-pyrazolone at the most favorable reaction conditions in order to examine the range and generality of this technique. Table 4 provides a summary of the findings. Different aromatic aldehydes containing both electron-withdrawing and electron-donating groups, including OH, OCH$_3$, NO$_2$, and CH$_3$, generated their respective derivatives in good to exceptional yields, according to the experimental data. The calculation of turnover number (TON) and turnover frequencies (TOF) of 4,4′-(arylmethylene)bis(1H-pyrazole-5-ol) derivatives is shown in Table 4.

3.2.2 Suggested mechanism

In the comparison of catalytic activity of poly(aniline-co-melamine) with nanoparticle MnFe$_2$O$_4$ in Table 1, the result showed that poly(aniline-co-melamine) is more active than MnFe$_2$O$_4$. Therefore, it seems that the amine group on the polymer will be the active site of the catalyst. A possible mechanism showed in (Figure 9). The initial deprotonation of 3-methyl-1-phenyl-1H-pyrazole-5-ol by amino groups in catalyst and then Knoevenagel condensation on the carbonyl group of the aldehyde that activated by ammonium ion. Then by removing H$_2$O, intermediate (I) is prepared. The reaction is followed by deprotonation of 3-methyl-1-phenyl-1H-pyrazole-5-ol, then Michael's addition of the resulted anion to intermediate 1 affords 2, and the product is obtained by tautomerization.

Here, it is described how to make the alkylene-bridging bis 4,4'-(arylmethylene)bis(3-methyl-1H-pyrazole-5-ols) derivative via a simple multicomponent reaction. To create a

TABLE 4 Synthesis of 4,4′-(arylmethylene)bis(1H-pyrazole-5-ol) derivatives.[a]

Entry	Product	Code	Time (Min.)	Yield %	TON	TOF X 10^{-3}(h^{-1})	M.p/°C		Ref
							Observed	Reported	
1		5a	20	95	3,518	10.6	171–173	173–174	Jahanshahi and Akhlaghinia, (2017)
2		5b	15	96	3,555	14.2	212–215	205–207	Jahanshahi and Akhlaghinia, (2017)
3		5c	25	93	3,444	8.4	203–205	202–204	Jahanshahi and Akhlaghinia, (2017)
4		5d	20	96	3,555	10.7	173–175	172–174	Jahanshahi and Akhlaghinia, (2017)
5		5e	10	96	3,555	22.2	223–225	230–232	Zolfigol et al. (2015)

TABLE 4 (*Continued*) Synthesis of 4,4′-(arylmethylene)bis(1*H*-pyrazole-5-ol) derivatives.[a]

Entry	Product	Code	Time (Min.)	Yield %	TON	TOF X 10^{-3}(h^{-1})	M.p/°C		Ref
							Observed	Reported	
6		5f	15	92	3,407	13.6	150–152	148–149	Jahanshahi and Akhlaghinia, (2017)
7		5g	30	95	3,518	7.0	195–197	194–196	Shabalala et al. (2020)
8		5h	30	94	3,481	6.9	155–157	153–155	Shabalala et al. (2020)
9		5i	25	96	3,555	8.6	206–208	205–207	Zolfigol et al. (2015)
10		5j	30	92	3,407	6.8	205–207		
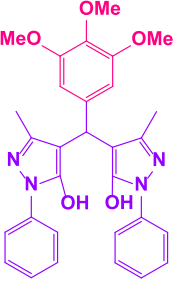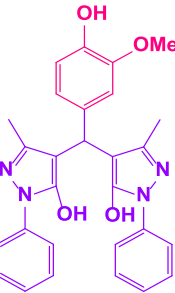
TABLE 4 (*Continued*) Synthesis of 4,4′-(arylmethylene)bis(1*H*-pyrazole-5-ol) derivatives.[a]

Entry	Product	Code	Time (Min.)	Yield %	TON	TOF X $10^{-3}(h^{-1})$	M.p/°C		Ref
							Observed	Reported	
11		**5k**	20	90	3,333	10.1	212–214	210–212	Jahanshahi and Akhlaghinia, (2017)
12		**5l**	10	95	3,518	21.9	226–228	227–229	Jahanshahi and Akhlaghinia, (2017)
13		**5m**	15	94	3,481	13.9	233–235	235–237	Jahanshahi and Akhlaghinia, (2017)
14		**5n**	30	90	3,333	6.6	159–161	159–160	Jahanshahi and Akhlaghinia, (2017)
15		**5o**	25	92	3,407	10.32	214–215	212–213	Zolfigol et al. (2015)
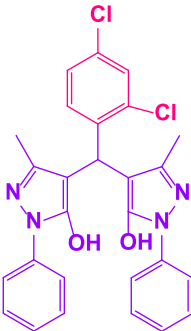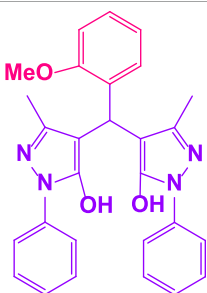
(Continued on following page)

TABLE 4 (*Continued*) Synthesis of 4,4'-(arylmethylene)bis(1*H*-pyrazole-5-ol) derivatives.[a]

Entry	Product	Code	Time (Min.)	Yield %	TON	TOF X $10^{-3}(h^{-1})$	M.p/°C		Ref
							Observed	Reported	
16		5P	30	90	3,333	6.6	190–191	185–188	Hasaninejad et al. (2011)
17		5q	70	94	3,481	3.1	194–196	193–193	Shabalala et al. (2020)
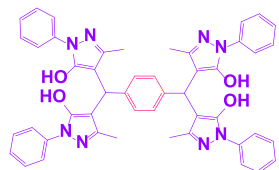
[a]Reaction conditions: aldehyde (1 mmol), 3-methyl-1-phenyl-1*H*-pyrazol-5-ol (2 mmol), and EtOH (5 ml) and Poly(aniline-*co*-melamine)@MnFe$_2$O$_4$ (0.05) at room temperature conditions.
The bold value row showed the best condition.
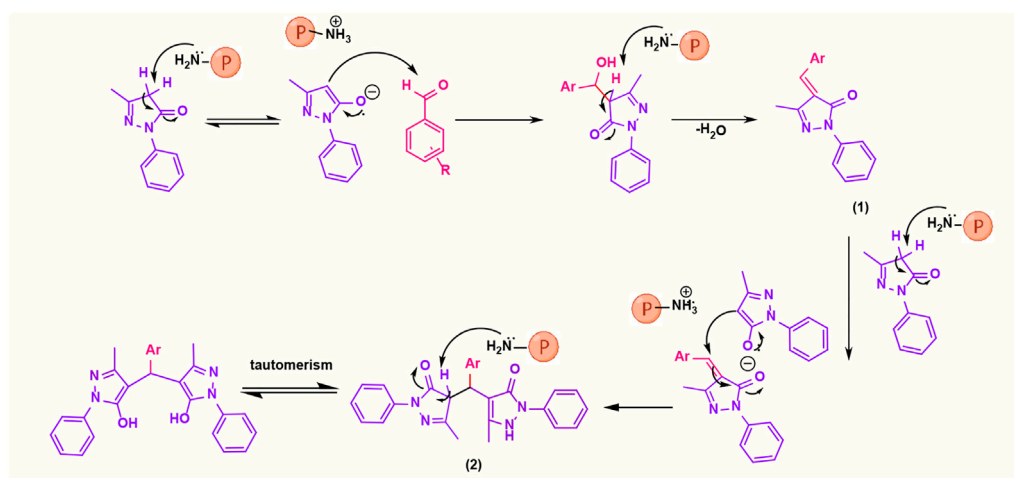
FIGURE 9
Suggested mechanistic scheme for the synthesis of 4,4'-(arylmethylene)bis(1*H*-pyrazole-5-ol) derivatives catalyzed by poly(aniline-*co*-melamine)@Mn(Fe$_2$O$_4$). ℗ represents polymer-based catalyst.

bifunctional aldehyde, dibromohexane (1 eq) and 2-hydroxybenzaldehyde (2 eq) were mixed. In the presence of poly(aniline-*co*-melamine)@MnFe$_2$O$_4$ as a catalyst, the resulting dialdehyde was condensed with the proper quantities of 3-methyl-1-phenyl-5-pyrazolone to produce bis 4,4'-(arylmethylene)bis (3-methyl-1*H*-pyrazole-5-ols) (Figure 10).

3.2.3 Recovery

The possibility of reusing and recycling the catalyst for the production of 6-mino-3-methyl-1,4-diphenyl-1,4-dihydropyrano[2,3-*c*]pyrazole-5-carbonitrile (4a) was investigated. The catalyst was recovered after conducting the reaction of benzaldehyde, 3-methyl-1-phenyl-
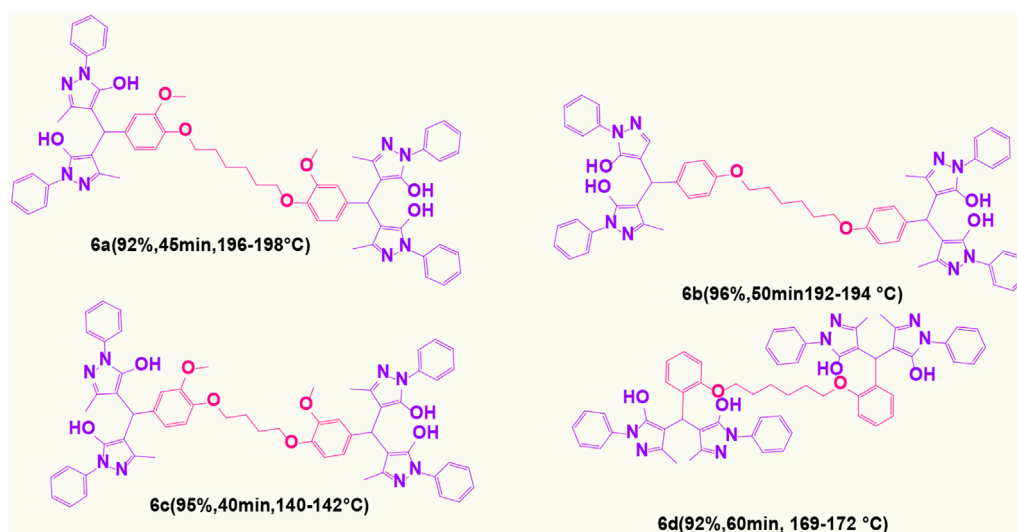
FIGURE 10
The structure of bis-4,4′-(arylmethylene)-bis-(3-methyl-1*H*-pyrazole-5-ols).
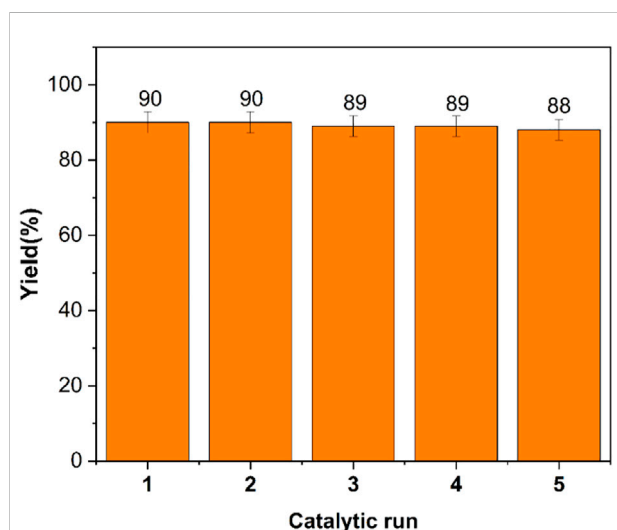
FIGURE 11
Reusability of poly(aniline-*co*-melamine)@MnFe$_2$O$_4$ in the synthesis 6- mino-3-methyl-1,4-diphenyl-1,4-dihydropyrano [2,3-*c*]pyrazole-5-carbonitrile (4a).

1*H*-pyrazole-5-ol, and malononitrile at the conditions specified in the experimental section. The catalyst was separated by an external magnet after adding hot ethanol to the reaction mixture. The catalyst was rinsed in ethanol (5 ml) and dried at low pressure. The catalyst was then re-fed into the reaction, as seen in Figure 11, where it continued to display good activity for the fifth time.

3.2.4 Antioxidant activity

The antioxidant activity of synthesized 4,4′-(arylmethylene) bis(1*H*-pyrazole-5-ols), bis 4,4′(arylmethylene) bis(3-methyl-1*H*-pyrazole-5-ols) and 1,4-dihydropyrano[2,3-*c*]pyrazoles were investigated using the 2,2-diphenyl-1-picrylhydrazyl (DPPH) scavenging model (Figure 12). The antioxidant activity of 22 synthesized derivatives was compared with ascorbic acid (vitamin c). Results showed that the antioxidant activity of synthesized derivatives after 60 min in an ethanolic solution of DPPH was between 70% and 98%. In addition, the antioxidant activity of ascorbic acid as a standard model was reported 96% (Janani et al., 2020) (Janani et al., 2020). These results showed that the synthesized derivatives can have good potential to be used in medicines or supplements with antioxidant properties.

3.2.5 *In*-vitro anticancer study

Anticancer study was evaluated against colon cancer (HCT116) and normal (L929) cell lines within 24–48 h and results were reported as the percent growth of the treated cells when compared to the untreated control cells (Figure 13).

After 24 h of exposure to colon cancer cells (Figure 13A) 6c and 4q samples showed significant toxicity in 25 μg/ml and higher doses. Other samples (5i, 5j, 5q, 4d, 4o, and 4l) had toxicity in 12.5 μg/ml and higher doses. After 48 h (Figure 13B), the 4q sample showed significant toxicity in 50 μg/ml and higher doses. On the other hand, 6c, 5i, and 5j samples had significant toxicity in 25 μg/ml and higher doses. Other samples (5q, 4l, 4o, and 4d) showed considerable toxicity in 12.5 μg/ml and higher doses. These results show that the tested dervatives have good
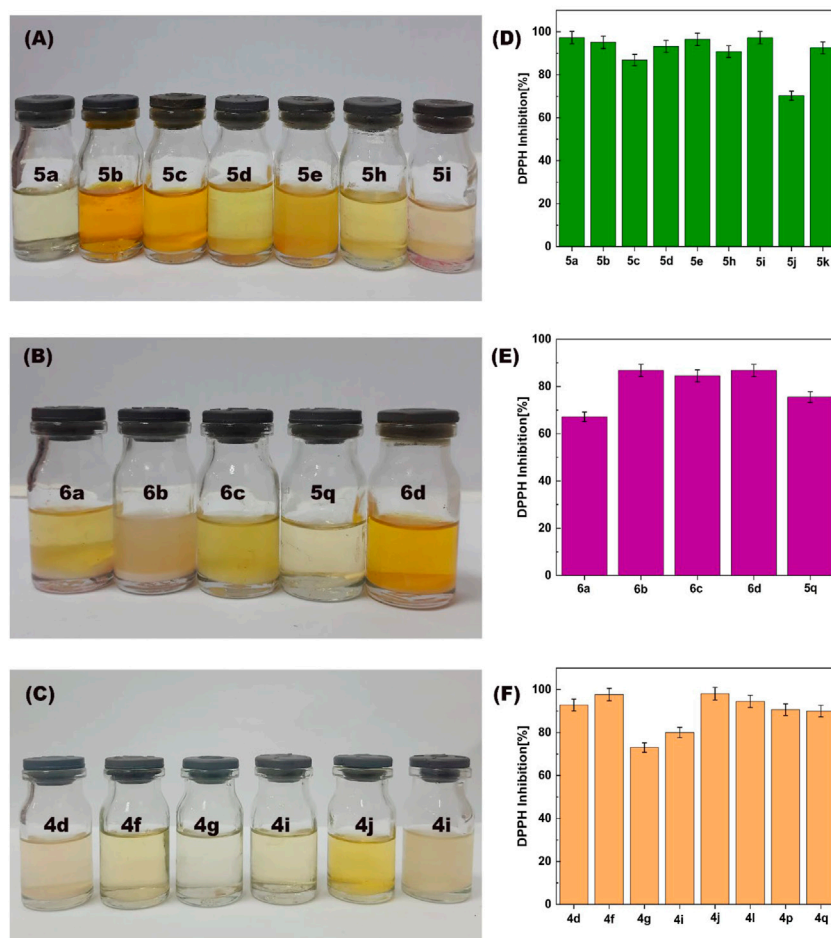
FIGURE 12
The photographs **(A–C)** and the histograms **(D–F)** of the antioxidant activity of synthesized of 1,4-dihydropyrano[2,3-c]pyrazoles (4q, 4f, 4g, 4i, 4d, and 4l), 4,4′-(arylmethylene)bis(1H-pyrazole-5-ol) (5a, 5b, 5c, 5d, 5e, 5h, 5i and 5q), bis 4,4′-(arylmethylene)bis(3-methyl-1H-pyrazol-5-ols) (6a, 6b, 6c, and 6d) derivatives.
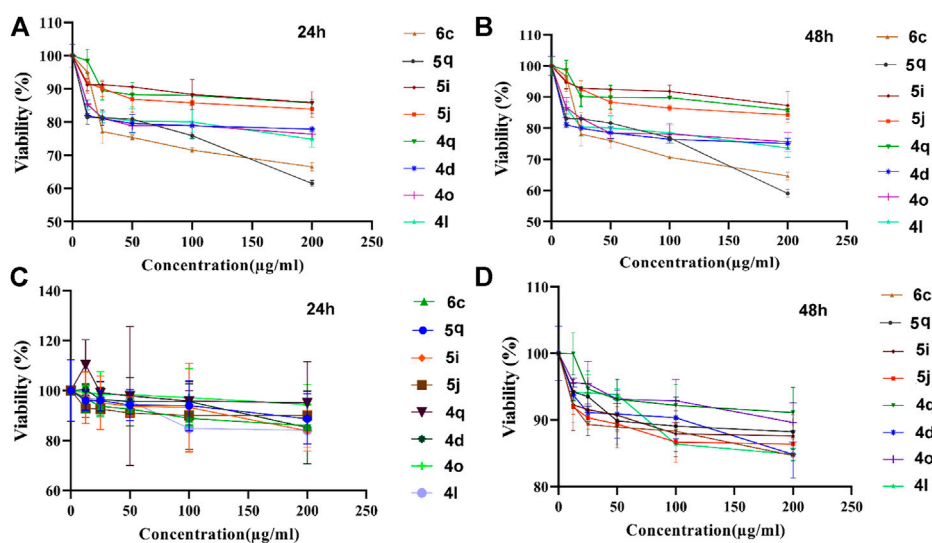
FIGURE 13
Anticancer activity of 1,4-dihydropyrano[2,3-c]pyrazoles (4q, 4d, 4o, 4l), 4,4′-(arylmethylene)bis(1H-pyrazole-5-ol) (5i, 5j, 5q), bis 4,4′-(arylmethylene)bis(3-methyl-1H-pyrazol-5-ols) (6c) derivatives against HCT116 **(A,B)** and L929 **(C,D)** cell lines.

potential for destroying cancer cells and can be used in drug compounds.

For better comparison, the normal cell line was also exposed to tested samples and results showed that after 24 h (Figure 13C), no considerable toxicity was observed for 25 μg/ml and lower doses for all samples. 5j sample was toxic in 50 μg/ml and higher doses. In addition, 6c and 4l samples showed significant toxicity in 100 μg/ml and higher doses. 5q, 5i, and 4d samples were toxic only in 200 μg/ml concentration. 4q and 4o samples did not cause toxicity in any of the applied concentrations.

After 48 h (Figure 13D), no considerable toxicity was observed in the 12.5 μg/ml concentration. 6c, 5i, 5j, and 4d samples showed significant toxicity in 25 μg/ml and higher doses. 5q and 4q samples showed significant toxicity in 50 μg/ml and higher doses. 4l sample was toxic in 100 μg/ml and higher doses. 4o samples were toxic only in 200 μg/ml concentration.

Results showed that the most effective anticancer agents were 5q and 6c samples which lead to ~30%–40% lethality in the highest applied dose (200 μg/ml). This concentration is relatively higher than conventional anticancer drugs. Two standard chemotherapeutic drugs commonly used in the treatment of colorectal cancer are 5-Fluorouracil (5-FU), and oxaliplatin (OXA) (Manoochehri et al., 2022). The IC50 for 5-FU in different colorectal cancer cell lines including HCT116 (used in this study) reported in a range between 0.6 and 4 μg/ml (Varghese et al., 2019). In a study performed by Yang et al. (2019), IC50 for 5-FU resistant HCT116 and HT29 colorectal cancer cell lines was 12.5 ± 1.4 μg/ml and 11.5 ± 1.5 μg/ml, respectively. They showed that IC50 of oxaliplatin in parental HCT-116 and OXA-resistant HCT116 cells was 9.18 and 70.01 μg/ml, respectively (Yang et al., 2019). However, chemical anticancer drugs have considerable toxicity against body normal cells owing to a lack of specificity (Sarfjoo et al., 2022), but 5q sample dose does not have considerable toxicity against normal cells in lower than 200 μg/ml doses in time points of 24 h.

4 Conclusion

A magnetic poly(aniline-*co*-melamine)@MnFe$_2$O$_4$ nanocomposite was prepared from poly(aniline-*co*-melamine) and manganese ferrite nanoparticles in two steps and was used as a catalyst in the synthesis of 1,4-dihydropyrano[2,3-*c*]pyrazoles, and 4,4′-(arylmethylene)bis(1*H*-pyrazole-5-ols) *via* one-pot, three-component condensation. FESEM image of nanocomposite showed disordered rod-like structures with an average particle size of 50 nm. In addition, TGA analysis showed high thermal stability for magnetic nanocomposite. The poly(aniline-*co*-melamine)@MnFe$_2$O$_4$ nanocatalyst showed great catalytic performance in the synthesis of 1,4-dihydropyrano[2,3-*c*]pyrazoles, 4,4′-(arylmethylene)

bis(1*H*-pyrazole-5-ols) and new alkylene bridging bis 4,4′-(arylmethylene)bis(1*H*-pyrazole-5-ols) derivatives. The maximum yield of the 1,4-dihydropyrano[2,3-c]pyrazoles, 4,4′-(arylmethylene)bis(1H-pyrazole-5-ols)and 4,4′-(arylmethylene)bis(1H-pyrazole-5-ols) with 0.05 g of poly(aniline-co-melamine)@MnFe$_2$O$_4$ as nanocatalyst were obtained 95% in 15 min, 96% in 15 min, and 96% in 50 min, respectively.

The maximum yield of the 1,4-dihydropyrano[2,3-c]pyrazoles with 0.05 g of poly(aniline-comelamine)@MnFe2O4 at 40°C in EtOH/ water as a green solvent and mild conditions were obtained at 95 % in 15 min,. Also, tthe maximum yield of the 4,4′-(arylmethylene)bis(1H-pyrazole-5-ols) with 0.05 g of catalyst at r.t conditions in EtOH was obtained at 96 % in 15 min. and the maximum yield of the bis 4,4′-(arylmethylene)bis(1H-pyrazole-5-ols) with 0.05 g of catalyst at r.t conditions in EtOH was obtained at 96 % in 50 min. . Moreover, the poly(aniline-*co*-melamine)@MnFe$_2$O$_4$ nanocatalyst was separated easily from the reaction mixture by an external magnet. The catalyst could be reused at least five times, without a substantial loss of catalytic activity. The presence of amine and hydroxyl groups in the produced 1,4-dihydropyrano[2,3-*c*]pyrazoles and 4,4′-(arylmethylene)bis(1*H*-pyrazole-5-ols) resulted in antioxidant activity ranging from 70% to 98%. In addition, 4,4′-(arylmethylene)bis(1*H*-pyrazole-5-ol) derivatives and 1,4-dihydropyrano[2,3-*c*]pyrazoles showed good potential for destroying colon cancer cell line.

4.1 Spectroscopic data

4.1.1 6- mino-3-methyl-1,4-diphenyl-1,4-dihydropyrano[2,3-c]pyrazole-5-carbonitrile (4a)

White powder, m. p. 169°C–172°C (Rep. 168°C–169°C) (Vafajoo et al., 2015); FTIR (KBr) υ$_{max}$/cm^{-1}: 3,447, 3,321, 2,921, 2199,1660, 1,560; ^{1}H NMR (300 MHz, DMSO-d_6): δ = 1.78 (s, 3H, CH$_3$), 4.68 (s, 1H, benzilic), 7.23-7.35 (m, 8H, aromatic), 7.50 (t, 2H, J = 7.5 Hz, aromatic),7.80 (d, 2H, J = 7.8 Hz, aromatic) ppm (Supplementary Figure S1).

4.1.2 6-amino-4-(4-chlorophenyl)-3-methyl-1-phenyl-1,4-dihydropyrano[2,3-c]pyrazole-5-carbonitrile (4b)

White powder, m.p. 172°C–173°C (Rep. 174°C–176°C) (Vafajoo et al., 2015); FTIR (KBr) υ$_{max}$/cm^{-1}: 3,445, 3,322, 2,923, 2197,1663, 1,562; ^{1}H NMR (300 MHz, DMSO-d_6): δ = 1.80 (s, 3H, CH$_3$), 4.73 (s, 1H, benzilic), 7.28-7.35 (m, 5H, aromatic), 7.40-7.43 (m, 2H, aromatic), 7.50 (t, 2H, J = 7.5 Hz, aromatic), 7.79 (d, 2H, J = 7.8 Hz, aromatic) ppm (Supplementary Figure S2).

4.1.3 6-amino-3-methyl-4-(4-nitrophenyl)-1-phenyl-1,4-dihydropyrano[2,3-c]pyrazole-5-carbonitrile (4e)

White powder, m.p. 192°C–193°C (Rep. 190°C–195°C) (Vafajoo et al., 2015); FTIR (KBr) υ_{max}/cm^{-1}: 3,446, 3,332, 2,913, 2,193, 1,668, 1,552, 1,351; ^{1}H NMR (300 MHz, DMSO-d_6): $\delta = 1.80$ (s, 3H, CH$_3$), 4.93 (s, 1H, benzilic), 7.34-7.40 (m, 3H, aromatic), 7.51-7.60 (m, 4H, aromatic), 7.80 (d, 2H, $J = 6.6$ Hz, aromatic), 8.24 (d, 2H, $J = 6.9$ Hz, aromatic)ppm (Supplementary Figure S3).

4.1.4 6-amino-3-methyl-1-phenyl-4-(3,4,5-trimethoxyphenyl)-1,4-dihydropyrano[2,3-c]pyrazole-5-carbonitrile (4g)

White powder, m.p. 202°C–204°C (Rep. 200°C–203°C) (Jasim et al., 2022); FTIR (KBr) υ_{max}/cm^{-1}: 3,445, 3,342, 2,921, 2192,1661, 1,530, 1,210; ^{1}H NMR (300 MHz, DMSO-d_6): $\delta = 1.87$ (s, 3H, CH$_3$), 3.35 (s, 3H, OMe), 3.66 (s, 6H, OMe), 4.67 (s, 1H, benzilic), 6.65 (br, 2H, NH$_2$), 7.23-7.34 (m, 3H, aromatic), 7.46-7.51 (m, 2H, aromatic), 7.80 (d, 2H, $J = 7.80$ Hz, aromatic) ppm (Supplementary Figure S4).

4.1.5 6-amino-4-(3-ethoxy-4-hydroxyphenyl)-3-methyl-1-phenyl-1,4-dihydropyrano[2,3-c]pyrazole-5-carbonitrile (4j)

White powder, m.p. 172°C–173°C (Rep. 169°C–171°C) (Vafajoo et al., 2015); FTIR (KBr) υ_{max}/cm^{-1}: 3,445, 3,342, 2,921, 2192,1661, 1,530, 1,210; ^{1}H NMR (400 MHz, DMSO-d_6): $\delta = 1.31$ (t, 3H, $J = 8$ Hz, CH$_3$), 1.82 (s, 3H, CH$_3$), 3.98 (q, 2H, $J = 8$ Hz, OCH$_2$), 4.57 (s, 1H, benzilic), 6.62 (d.d, 1H, $= 8$ Hz, aromatic), 6.74-6.80 (m, 2H), 7.15 (br, 2H, NH$_2$), 7.32 (t.d, 1H, $J = 4$ Hz, aromatic), 7.49 (t, 2H, $J = 12$ Hz, aromatic), 7.79 (d.d, 2H, $J = 7.80$ Hz, aromatic) ppm (Supplementary Figure S5).

4.1.6 6-amino-3-methyl-4-(naphthalen-1-yl)-1-phenyl-1,4-dihydropyrano[2,3-c]pyrazole-5-carbonitril (4k)

White powder, m.p.240°C–242°C (Rep. 244°C–245°C) (Zolfigol et al., 2016); FTIR (KBr) υ_{max}/cm^{-1}: 3,447, 3,392, 2,911, 2,196, 1,662, 1,550; ^{1}H NMR (300 MHz, DMSO-d_6): $\delta = 2.30$ (s, 3H, CH$_3$), 5.61 (s, 1H, benzilic), 7.20-7.24 (m, 2H, aromatic), 7.40-7.55 (m, 5H, aromatic), 7.70-8.01 (m, 7H, aromatic) ppm (Supplementary Figure S6).

4.1.7 6-amino-3-methyl-1-phenyl-4-(thiophen-2-yl)-1,4-dihydropyrano[2,3-c]pyrazole-5-carbonitrile (4o)

White powder, m.p.168°C–170°C (Rep. 167°C–168°C) (Zolfigol et al., 2016); FTIR (KBr) υ_{max}/cm^{-1}: 3,447, 3,392, 2,911, 2,196, 1,662, 1,550; ^{1}HNMR(400 MHz, DMSO-d_6): $\delta = 1.93$ (s, 3H, CH$_3$), 5.10 (s, 1H, benzilic), 6.98-7.00 (m, 1H,aromatic), 7.08 (d.d, 1H, $J = 8$ Hz, aromatic), 7.32-7.35 (m, 2H, aromatic), 7.44 (d, 2H, $J = 4$ Hz), 7.50 (t, 1H, $J = 8$ Hz, aromatic), 7.79 (d.d, 2H, $J = 8$ Hz, aromatic) ppm (Supplementary Figure S7).

4.1.8 4,4′-((4-hydroxy-3-methoxyphenyl)methylene)bis(3-methyl-1-phenyl-1H-pyrazol-5-ol) (5i)

White powder, m.p.206°C–208°C (Rep. 206°C–207°C) (Zolfigol et al., 2015); FTIR (KBr) υ_{max}/cm^{-1}: 3,451, 3,286, 2,941, 1,617; ^{1}H NMR (300 MHz, DMSO-d_6): $\delta = 2.31$ (s, 6H, CH$_3$),3.14 (s, 3H, OCH$_3$), 4.85 (s, 1H, benzilic), 6.69 (br, 2H, aromatic), 6.86 (s, 1H, aromatic), 7.24 (t, 4H, $J = 7.2$ Hz, aromatic), 7.71 (d, 4H, $J = 7.5$ Hz, aromatic), 8.76(br, 1H, OH), 14.02 (br, 2H, OH) ppm (Supplementary Figure S8).

4.1.9 4,4′-(naphthalen-1-ylmethylene)bis(3-methyl-1-phenyl-1H-pyrazol-5-ol) (5k)

White powder, m.p.212°C–214°C (Rep. 210°C–212°C) (Jahanshahi and Akhlaghinia, 2017); FTIR (KBr) υ_{max}/cm^{-1}3420, 3,176, 2,940, 1619,1105; ^{1}H NMR (400 MHz, DMSO-d_6): $\delta = 2.30$ (s, 6H, CH$_3$), 5.62 (s, 1H, benzilic), 7.21-7.24 (m, 2H, aromatic), 7.41-7.55 (m, 7H, aromatic), 7.65-7.73 (m, 5H, aromatic), 7.93-8.02 (m, 2H, aromatic), 13.18 (br, 2H, OH) ppm (Supplementary Figure S9).

4.1.10 4,4′-((2-methoxyphenyl)methylene)bis(3-methyl-1-phenyl-1H-pyrazol-5-ol) (5o)

White powder, m.p.214°C–215°C (Rep. 212°C–213°C) (Jahanshahi and Akhlaghinia, 2017); FTIR (KBr) υ_{max}/cm^{-1}: 3,431, 3,176, 2,946, 1,621, 1,115 ^{1}H NMR (400 MHz, DMSO-d_6): $\delta = 2.30$ (s, 6H, CH$_3$), 3.38 (s, 3H, OCH$_3$), 5.21 (s, 1H, benzilic), 6.87-6.97 (m, 2H, aromatic), 7.15-7.28 (m, 3H, aromatic), 7.45 (t, 4H, $J = 7.8$ Hz, aromatic), 7.63 (d, 1H, $J = 6.6$ Hz, aromatic), 7.72 (d, 4H, $J = 7.8$ Hz, aromatic), 14.41 (br, 2H, OH) ppm (Supplementary Figure S10).

4.1.11 4,4′,4″,4‴-(((hexane-1,6-diylbis(oxy))bis(3-methoxy-4,1-phenylene))bis(methanetriyl)) tetrakis(3-methyl-1-phenyl-1H-pyrazol-5-ol) (6a)

White powder, m.p.196°C–198°C; FTIR (KBr) υ_{max}/cm^{-1}: 3,418, 3,228, 2,967, 1,609, 1,535; ^{1}H NMR (400 MHz, DMSO-d$_6$): $\delta = 1.43$ (br, 2H, CH$_2$, bridge), 1.68 (br, 2H, CH$_2$, bridge), 2.31 (s, 6H, CH$_3$), 3.64 (s, 3H, OCH$_3$), 3.88 (m, 2H, OCH$_2$, bridge), 4.87 (s, 1H, benzilic), 6.79-6.78 (m, 3H, aromatic), 7.24 (t, 2H, J = 7.2 Hz,aromatic), 7.44 (t, 4H, J = 8 Hz, aromatic), 7.70 (d, 4H, J = 7.6 Hz, aromatic), 14.03 (s, 1H, OH) ppm. ^{13}C NMR (100 MHz, DMSO-d$_6$): $\delta = 25.77$, 29.24, 33.35, 56.04, 56.50, 68.64, 112.38, 113.49, 119.84, 121.06, 126.04, 129.39, 135.42, 146.62, 147.07, and 149.09 ppm (Supplementary Figure S11).

4.1.12 4,4′-((4-((6-(4-((5-hydroxy-1-phenyl-1H-pyrazol-4-yl)(5-hydroxy-3-methyl-1-phenyl-1H-pyrazol-4-yl)methyl)phenoxy)hexyl)oxy)phenyl)methylene)bis(3-methyl-1-phenyl-1H-pyrazol-5-ol) (6b)

White powder, m.p.192°C–194°C; FTIR (KBr) υ_{max}/cm^{-1}: 3,423, 3,211, 2,973, 1,611, 1,528; ^{1}H NMR (400 MHz, DMSO-d$_6$): $\delta = 1.43$

(br, 2H, CH$_2$ bridge), 1.67 (br, 2H, CH$_2$ bridge), 2.30 (s, 6H, CH$_3$), 3.89 (t, 2H, J = 6.4 Hz, OCH$_2$ bridge), 4.88 (s, 1H, benzilic), 6.81 (d, 2H, J = 8.8 Hz, aromatic), 7.13 (d, 2H, J = 8.4 Hz, aromatic),7.24 (t, 2H, J = 7.2 Hz,aromatic), 7.43 (t, 4H, J = 7.6 Hz, aromatic), 7.70 (d, 4H, J = 7.6 Hz, aromatic), 13.94 (s, 1H, OH) ppm. ^{13}C NMR (100 MHz, DMSO-d$_6$): δ = 25.81, 29.16, 32.80, 56.50, 67.71, 114.48, 115.36, 120.96, 126.01, 128.60, 129.38, 132.28, 134.36, 146.64, and 157.39 ppm (Supplementary Figure S12).

4.1.13 4,4′,4″,4‴-(((butane-1,4-diylbis(oxy)) bis(3-methoxy-4,1-phenylene)) bis(methanetriyl)) tetrakis(3-methyl-1-phenyl-1H-pyrazol-5-ol) (6c)

White powder, m.p.140°C–142°C; FTIR (KBr) υ$_{max}$/cm^{-1}: 3,423, 3,236, 2,951, 1618,1103; ^{1}H NMR (400 MHz, DMSO-d$_6$): δ = 1.82 (br, 2H, CH$_2$ bridge), 2.31 (s, 6H, CH$_3$), 3.83 (s, 3H,OCH$_3$), 4.17 (br, 2H, OCH$_2$ bridge), 4.88 (s, 1H, benzilic), 6.78-6.88 (m, 3H, aromatic), 7.24 (t, 2H, J = 7.2 Hz, aromatic), 7.44 (t, 4H, J = 8 Hz, aromatic), 7.70 (d, 4H, J = 8 Hz, aromatic), 14.03 (s, 1H, OH) ppm. ^{13}C NMR (100 MHz, DMSO-d$_6$): δ = 25.72, 33.36, 55.98, 56.51, 38.45, 112.44, 113.51, 119.81, 121.06, 126.05, 129.39, 135.47, 146.65, 149.67, and 154.00 ppm (Supplementary Figure S13).

4.1.14 4,4′,4″,4‴-(((hexane-1,6-diylbis(oxy)) bis(2,1-phenylene))bis(methanetriyl))tetrakis(3-methyl-1-phenyl-1H-pyrazol-5-ol) (6d)

White powder, m.p.169°C–172°C; FTIR (KBr) υ$_{max}$/cm^{-1}: 3,422, 3,225, 2,963, 1,615, 1,541, ^{1}H NMR (400 MHz, DMSO-d$_6$): δ = 1.52 (br, 2H, CH$_2$ bridge), 1.79 (br, 2H, CH$_2$ bridge), 2.29 (s, 6H, CH$_3$), 4.01 (br, 2H, OCH$_2$ bridge), 5.25 (s, 1H, benzilic), 6.86 (t, 1H, J = 7.2 Hz,aromatic), 6.92 (d, 1H, J = 8.4 Hz, aromatic), 7.14 (t, 1H, J = 7.6 Hz,aromatic), 7.23 (t, 2H, J = 7.2 Hz, aromatic), 7.43 (t, 4H, J = 8 Hz, aromatic), 7.67-7.72 (m, 5H, aromatic), 14.23 (s, 1H, OH) ppm. ^{13}C NMR (100 MHz, DMSO-d$_6$): δ = 25.91, 27.61, 29.27, 56.50, 68.05, 11.86, 120.29, 121.07, 126.08, 127.76, 128.05, 129.37, 131.17, 146.43, and 155.41 ppm (Supplementary Figure S14).

4.1.15 4,4′,4″,4‴-(1,4-phenylenebis(methanetriyl)) tetrakis(3-methyl-1-phenyl-1H-pyrazol-5-ol) (6e)

White powder, m.p.194°C–196°C (Rep. 193°C–196°C) (Hasaninejad et al., 2011); FTIR (KBr) υ$_{max}$/cm^{-1}: 3,419, 3,229, 2,981, 1628,1105; ^{1}H NMR (400 MHz, DMSO-d$_6$): δ = 2.30 (s, 6H, CH$_3$), 4.89 (s, 1H, benzilic), 7.18 (s, 2H, aromatic), 7.24 (t,

2H, J = 6.8 Hz, aromatic), 7.42 (t, 4H, J = 7.6 Hz, aromatic), 7.68 (d, 4H, J = 8 Hz, aromatic), 14.07 (br, 2H, OH) ppm. ^{13}C NMR (100 MHz, DMSO-d$_6$): δ = 33.23, 66.82, 121.12, 126.16, 127.46, 129.36, 140.44, and 146.68 ppm (Supplementary Figure S15).

Data availability statement

The raw data supporting the conclusion of this article will be made available by the authors, without undue reservation.

Author contributions

SM experimented and wrote the manuscript. GH wrote the manuscript. SP and EN supervision and edited the manuscript. ES and HM examined the anticancer activity.

Conflict of interest

The authors declare that the research was conducted in the absence of any commercial or financial relationships that could be construed as a potential conflict of interest.

The reviewer AM declared a past co-authorship with the author EN to the handling editor.

Publisher's note

All claims expressed in this article are solely those of the authors and do not necessarily represent those of their affiliated organizations, or those of the publisher, the editors and the reviewers. Any product that may be evaluated in this article, or claim that may be made by its manufacturer, is not guaranteed or endorsed by the publisher.

Supplementary material

The Supplementary Material for this article can be found online at: https://www.frontiersin.org/articles/10.3389/fchem.2022.1046120/full#supplementary-material

References

Al-Hasani, T. J., Mihsen, H. H., Hello, K. M., and Adam, F. (2017). Catalytic esterification via silica immobilized p-phenylenediamine and dithiooxamide solid catalysts. *Arab. J. Chem.* 10, S1492–S1500. doi:10.1016/j.arabjc.2013.04.030

Alizadeh, E., and Baseri, H. (2022). Photocatalytic degradation of sumatriptan succinate by ZnO, Fe doped ZnO and TiO2-ZnO nanocatalysts. *Mat. Chem. Horizons* 1, 7–21. doi:10.22128/mch.2022.534.1002

Amir, M., Kumar, H., and Khan, S. A. (2008). Synthesis and pharmacological evaluation of pyrazoline derivatives as new anti-inflammatory and analgesic agents. *Bioorg. Med. Chem. Lett.* 18, 918–922. doi:10.1016/j.bmcl.2007.12.043

Bououdina, M., and Manoharan, C. (2020). Dependence of structure/morphology on electrical/magnetic properties of hydrothermally synthesised cobalt ferrite nanoparticles. *J. Magn. Magn. Mat.* 493, 165703. doi:10.1016/j.jmmm.2019.165703

Carta, D., Casula, M. F., Floris, P., Falqui, A., Mountjoy, G., Boni, A., et al. (2010). Synthesis and microstructure of manganese ferrite colloidal nanocrystals. *Phys. Chem. Chem. Phys.* 12, 5074–5083. doi:10.1039/b922646j

Dang, C., Mu, Q., Xie, X., Sun, X., Yang, X., Zhang, Y., et al. (2022). Recent progress in cathode catalyst for nonaqueous lithium oxygen batteries: A review. *Adv. Compos. Hybrid. Mat.* 5, 606–626. doi:10.1007/s42114-022-00500-8

Deraz, N. M., and Alarifi, A. (2012). Controlled synthesis, physicochemical and magnetic properties of nano-crystalline Mn ferrite system. *Int. J. Electrochem. Sci.* 7 (6), 5534–5543.

Ghahremanloo, A., Zare, E. N., Salimi, F., and Makvandi, P. (2022). Electroconductive and photoactive poly(phenylenediamine)s with antioxidant and antimicrobial activities for potential photothermal therapy. *New J. Chem.* 46, 6255–6266. doi:10.1039/d1nj06145c

Gu, Y., Pan, Z., Zhang, H., Zhu, J., Yuan, B., Pan, D., et al. (2020). Synthesis of high performance diesel oxidation catalyst using novel mesoporous AlLaZrTiOx mixed oxides by a modified sol-gel method. *Adv. Compos. Hybrid. Mat.* 3, 583–593. doi:10.1007/s42114-020-00193-x

Guo, J., Chen, Z., Abdul, W., Kong, J., Khan, M. A., Young, D. P., et al. (2021a). Tunable positive magnetoresistance of magnetic polyaniline nanocomposites. *Adv. Compos. Hybrid. Mat.* 4, 534–542. doi:10.1007/s42114-021-00242-z

Guo, J., Li, X., Liu, H., Young, D. P., Song, G., Song, K., et al. (2021b). Tunable magnetoresistance of core-shell structured polyaniline nanocomposites with 0-1- and 2-dimensional nanocarbons. *Adv. Compos. Hybrid. Mat.* 4, 51–64. doi:10.1007/s42114-021-00211-6

Hajizadeh, Z., and Maleki, A. (2018). Poly(ethylene imine)-modified magnetic halloysite nanotubes: A novel, efficient and recyclable catalyst for the synthesis of dihydropyrano[2, 3-c]pyrazole derivatives. *Mol. Catal.* 460, 87–93. doi:10.1016/J.MCAT.2018.09.018

Hasaninejad, A., Zare, A., Shekouhy, M., and Golzar, N. (2011). Efficient synthesis of 4, 4'-(Arylmethylene)-bis(3-methyl-1-phenylpyrazol-5- ol) derivatives in PEG-400 under catalyst-free conditions. *Org. Prep. Proced. Int.* 43, 131–137. doi:10.1080/00304948.2010.526827

Hassanzadeh-Afruzi, F., Heidari, G., and Maleki, A. (2022). Magnetic nanocomposite Hydrogel based on Arabic gum for Remediation of lead(II) from Contaminated water. *Mat. Chem. Horizons* 1, 107–122. doi:10.22128/mch.2022.570.1013

Hu, X., Mandika, C., He, L., You, Y., Chang, Y., Wang, J., et al. (2019). Construction of Urokinase-Type Plasminogen activator Receptor-targeted Heterostructures for efficient photothermal Chemotherapy against Cervical cancer to Achieve simultaneous anticancer and Antiangiogenesis. *ACS Appl. Mat. Interfaces* 11, 39688–39705. doi:10.1021/acsami.9b15751

Hule, R. A., and Pochan, D. J. (2007). Polymer nanocomposites for biomedical applications. *MRS Bull.* 32, 354–358. doi:10.1557/mrs2007.235

Islam, K., Haque, M., Kumar, A., Hoq, A., Hyder, F., and Hoque, S. M. (2020). Manganese ferrite nanoparticles (MnFe2 O4): Size dependence for hyperthermia and negative/positive contrast enhancement in MRI. *Nanomaterials* 10, 2297–2323. doi:10.3390/nano10112297

Jahanshahi, R., and Akhlaghinia, B. (2017). Sulfonated Honeycomb coral (HC-SO3H): A new, green and highly efficient heterogeneous catalyst for the rapid one-pot pseudo-five component synthesis of 4, 4'-(aryl methylene) bis(3-methyl-1H-pyrazol-5-ol)s. *Chem. Pap.* 71, 1351–1364. doi:10.1007/s11696-016-0127-y

Janani, N., Zare, E. N., Salimi, F., and Makvandi, P. (2020). Antibacterial tragacanth gum-based nanocomposite films carrying ascorbic acid antioxidant for bioactive food packaging. *Carbohydr. Polym.* 247, 116678. doi:10.1016/j.carbpol.2020.116678

Jasim, S. A., Al-Awsi, G. R. L., Qasim, M. T., Tukhtaev, J., and Al-Gazally, M. E. (2022). Synthesis and evaluation anticancer activity of new novel Bismuth-metal organic framework as efficient and reusable nanocatalyst. *Res. Square*, 1–15. Preprint. doi:10.21203/rs.3.rs-1806840/v1

Jazzar, A., Alamri, H., Malajati, Y., Mahfouz, R., Bouhrara, M., and Fihri, A. (2021). Recent advances in the synthesis and applications of magnetic polymer nanocomposites. *J. Ind. Eng. Chem.* 99, 1–18. doi:10.1016/j.jiec.2021.04.011

Kalia, S., Kango, S., Kumar, A., Haldorai, Y., Kumari, B., and Kumar, R. (2014). Magnetic polymer nanocomposites for environmental and biomedical applications. *Colloid Polym. Sci.* 292, 2025–2052. doi:10.1007/s00396-014-3357-y

Kamalzare, M. (2022). "Effectiveness of morphology and size," in *Heterogeneous micro and Nanoscale composites for the Catalysis of organic reactions* (Elsevier), 91–111.

Larsen, J. S., Zahran, M. A., Pedersen, E. B., and Nielsen, C. (1999). Synthesis of triazenopyrazole derivatives as potential inhibitors of HIV-1. *Monatsh. Fuer. Chem.* 130, 1167–1173. doi:10.1007/pl00010295

Lian, Y., Wang, L., Cao, J., Liu, T., Xu, Z., Yang, B., et al. (2021). Recent advances on the magnetic nanoparticle–based nanocomposites for magnetic induction hyperthermia of tumor: A short review. *Adv. Compos. Hybrid. Mat.* 4, 925–937. doi:10.1007/s42114-021-00373-3

Manoochehri, H., Tanzadehpanah, H., Taherkhani, A., and Jalali, A. (2022). A Gene expression signature to Predict Chemotherapy Response of colorectal cancer Patients: Systems Biology analysis on Transcriptomics data and experimental Validation. *J. Appl. Biotechnol. Rep.* 9, 657–670.

Maroufi, P., Najafi Moghadam, P., and Vahabi, H. (2020). New nitrogen-rich flame retardant based on conductive poly(aniline-co-melamine). *React. Funct. Polym.* 150, 104548. doi:10.1016/j.reactfunctpolym.2020.104548

Massart, R. (1981). Preparation of aqueous magnetic liquids in Alkaline and acidic media. *IEEE Trans. Magn.* 17, 1247–1248. doi:10.1109/TMAG.1981.1061188

Molaei, S., and Javanshir, S. (2018). Preparation, characterization and use of new lignocellulose-based bio nanocomposite as a heterogeneous catalyst for sustainable synthesis of pyrimido benzazoles. *Green Chem. Lett. Rev.* 11, 275–285. doi:10.1080/17518253.2018.1484180

Movagharnezhad, N., Ehsanimehr, S., and Najafi Moghadam, P. (2022). Synthesis of poly (N-vinylpyrrolidone)-grafted-Magnetite Bromoacetylated Cellulose via ATRP for drug delivery. *Mat. Chem. Horizons* 1, 89–98. doi:10.22128/mch.2022.545.1004

Nezhad, S. M., Pourmousavi, S. A., Zare, E. N., Heidari, G., and Makvandi, P. (2022). Magnetic sulfonated melamine-Formaldehyde Resin as an efficient catalyst for the synthesis of antioxidant and antimicrobial pyrazolone derivatives. *Catalysts* 12 (6), 626. doi:10.3390/catal12060626

Özdemir, Z. G., Kılıç, M., Karabul, Y., Mısırlıoğlu, B. S., Çakır, Ö., and Kahya, N. D. (2020). A transition in the electrical conduction mechanism of CuO/CuFe2O4 nanocomposites. *J. Electroceram.* 44, 1–15. doi:10.1007/s10832-019-00194-3

Parajuli, R. R., Pokhrel, P., Tiwari, A. K., and Banerjee, J. (2013). Pharmacological activities of pyrazolone derivatives. *J. Appl. Pharm. Res.* 1 (1), 05–13.

Park, H. J., Lee, K., Park, S. J., Ahn, B., Lee, J. C., Cho, H. Y., et al. (2005). Identification of antitumor activity of pyrazole oxime ethers. *Bioorg. Med. Chem. Lett.* 15, 3307–3312. doi:10.1016/j.bmcl.2005.03.082

Philippova, O., Barabanova, A., Molchanov, V., and Khokhlov, A. (2011). Magnetic polymer beads: Recent trends and developments in synthetic design and applications. *Eur. Polym. J.* 47, 542–559. doi:10.1016/j.eurpolymj.2010.11.006

Pimenova, E. V., and Voronina, E. V. (2001). Antimicrobial activity of pyrazoles and pyridazines obtained by interaction of 4-aryl-3-arylhydrazono-2, 4-dioxobutanoic acids and their esters with hydrazines. *Pharm. Chem. J.* 35, 602–604. doi:10.1023/A:1015141710100

Qin, H., Yang, Y., Shi, W., and She, Y. (2021). Heterogeneous Fenton degradation of ofloxacin catalyzed by magnetic nanostructured MnFe 2 O 4 with different morphologies. *Environ. Sci. Pollut. Res. Int.* 28 (21), 26558–26570. doi:10.1007/s11356-021-12548-y

Sarfjoo, M. R., Shad, A., Hassanpour, M., and Varma, R. (2022). An Overview on new anticancer drugs approved by food and drug Administration: Impending Economic and environmental Challenges. *Mat. Chem. Horizons* in press. doi:10.22128/mch.2022.588.1019

Shaabani, A., Seyyedhamzeh, M., Maleki, A., Behnam, M., and Rezazadeh, F. (2009). Synthesis of fully substituted pyrazolo[3, 4-b]pyridine-5-carboxamide derivatives via a one-pot four-component reaction. *Tetrahedron Lett.* 50, 2911–2913. doi:10.1016/j.tetlet.2009.03.200

Shabalala, N. G., Kerru, N., Maddila, S., van Zyl, W. E., and Jonnalagadda, S. B. (2020). Ultrasound-mediated catalyst-free protocol for the synthesis of bis-3-methyl-1-phenyl-1H-pyrazol-5-ols in aqueous ethanol. *Chem. Data Collect.* 28, 100467. doi:10.1016/j.cdc.2020.100467

Soares, S. F., Fateixa, S., Trindade, T., and Daniel-da-Silva, A. L. (2022). A versatile synthetic route towards gelatin-silica hybrids and magnetic composite colloidal nanoparticles. *Adv. Compos. Hybrid. Mat.* 5, 884–898. doi:10.1007/s42114-021-00386-y

Stevens, P. D., Fan, J., Gardimalla, H. M. R., Yen, M., and Gao, Y. (2005). Superparamagnetic nanoparticle-supported catalysis of Suzuki cross-coupling reactions. *Org. Lett.* 7, 2085–2088. doi:10.1021/ol050218w

Vafajoo, Z., Hazeri, N., Maghsoodlou, M. T., and Veisi, H. (2015). Electro-catalyzed multicomponent transformation of 3-methyl-1-phenyl-1H-pyrazol-5(4H)-one to 1, 4-dihydropyrano[2, 3-c]pyrazole derivatives in green medium. *Chin. Chem. Lett.* 26, 973–976. doi:10.1016/j.cclet.2015.04.016

Varghese, V., Magnani, L., Harada-Shoji, N., Mauri, F., Szydlo, R. M., Yao, S., et al. (2019). FOXM1 modulates 5-FU resistance in colorectal cancer through regulating TYMS expression. *Sci. Rep.* 9, 1505–1516. doi:10.1038/s41598-018-38017-0

Xu, D., Huang, G., Guo, L., Chen, Y., Ding, C., and Liu, C. (2022). Enhancement of catalytic combustion and thermolysis for treating

polyethylene plastic waste. *Adv. Compos. Hybrid. Mat.* 5, 113–129. doi:10.1007/s42114-021-00317-x

Yang, C., Pan, Y., and Deng, S. P. (2019). Downregulation of lncRNA CCAT1 enhances 5-fluorouracil sensitivity in human colon cancer cells. *BMC Mol. cell Biol.* 20, 9–11. doi:10.1186/s12860-019-0188-1

Yildirim, I., Özdemir, N., Akçamur, Y., Dinçer, M., and Andaç, Ö. (2005). 4-Benzoyl-1, 5-diphenyl-1H-pyrazole-3-carboxylic acid methanol solvate. *Acta Crystallogr. Sect. E Struct. Rep. Online* 61, 256–258. doi:10.1107/S1600536804034348

Zhu, Y., Stubbs, L. P., Ho, F., Liu, R., Ship, C. P., Maguire, J. A., et al. (2010). Magnetic nanocomposites: A new Perspective in catalysis. *ChemCatChem* 2, 365–374. doi:10.1002/cctc.200900314

Zipare, K., Dhumal, J., Bandgar, S., Mathe, V., and Shahane, G. (2015). Superparamagnetic manganese ferrite nanoparticles: Synthesis and magnetic properties. *J. Nanosci. Nanoeng.* 1, 178–182.

Zolfigol, M. A., Ayazi-Nasrabadi, R., Baghery, S., Khakyzadeh, V., and Azizian, S. (2016). Applications of a novel nano magnetic catalyst in the synthesis of 1, 8-dioxo-octahydroxanthene and dihydropyrano[2, 3-c]pyrazole derivatives. *J. Mol. Catal. A Chem.* 418–419, 54–67. doi:10.1016/j.molcata.2016.03.027

Zolfigol, M. A., Ayazi-Nasrabadi, R., and Baghery, S. (2015). Synthesis and characterization of two novel biological-based nano organo solid acids with urea moiety and their catalytic applications in the synthesis of 4, 4'-(arylmethylene)bis(1H-pyrazol-5-ol), coumarin-3-carboxylic acid and cinnamic acid derivatives under mild and green conditions. *RSC Adv.* 5, 71942–71954. doi:10.1039/c5ra14001c

Zolfigol, M. A., Ayazi-Nasrabadi, R., and Baghery, S. (2015). Synthesis and characterization of two novel biological-based nano organo solid acids with urea